Published in final edited form as:
Mol Cell Neurosci. 2019 September 01; 99: 103390. doi:10.1016/j.mcn.2019.103390.

Amyloid-beta impairs insulin signaling by accelerating autophagy-lysosomal degradation of LRP-1 and IR-β in blood-brain barrier endothelial cells *in vitro* and in 3XTg-AD mice

Chaitanya Chakravarthi Gali[a], **Elham Fanaee-Danesh**[a], **Martina Zandl-Lang**[a], **Nicole Maria Albrecher**[a], **Carmen Tam-Amersdorfer**[a], **Anika Stracke**[a], **Vinay Sachdev**[b], **Florian Reichmann**[c], **Yidan Sun**[a], **Afrim Avdili**[a], **Marielies Reiter**[a], **Dagmar Kratky**[b,e], **Peter Holzer**[c], **Achim Lass**[d,e], **Karunya K. Kandimalla**[f], **Ute Panzenboeck**[a,e,*]

[a]Division of Immunology and Pathophysiology, Otto Loewi Research Center for Vascular Biology, Immunology and Inflammation, Medical University of Graz, Graz, Austria

[b]Division of Molecular Biology and Biochemistry, Gottfried Schatz Research Center for Cell Signaling, Metabolism and Aging, Medical University of Graz, Graz, Austria

[c]Division of Pharmacology, Otto Loewi Research Center for Vascular Biology, Immunology and Inflammation, Medical University of Graz, Graz, Austria

[d]Institute of Molecular Biosciences, University of Graz, Graz, Austria

[e]BioTechMed-Graz, Graz, Austria

[f]College of Pharmacy, Department of Pharmaceutics, University of Minnesota, Minneapolis, MN, USA

Abstract

Aberrant insulin signaling constitutes an early change in Alzheimer's disease (AD). Insulin receptors (IR) and low-density lipoprotein receptor-related protein-1 (LRP-1) are expressed in brain capillary endothelial cells (BCEC) forming the blood-brain barrier (BBB). There, insulin may regulate the function of LRP-1 in Aβ clearance from the brain. Changes in IR-β and LRP-1 and insulin signaling at the BBB in AD are not well understood. Herein, we identified a reduction in cerebral and cerebrovascular IR-β levels in 9-month-old male and female 3XTg-AD ($PS1_{M146V}$, APP_{Swe}, and tau_{P301L}) as compared to NTg mice, which is important in insulin mediated signaling responses. Reduced cerebral IR-β levels corresponded to impaired insulin signaling and LRP-1

*Corresponding author at: Division of Immunology and Pathophysiology, Otto Loewi Research Center for Vascular Biology, Immunology and Inflammation, Medical University of Graz, Heinrichstrasse 31a, A-8010 Graz, Austria. ute.panzenboeck@medunigraz.at (U. Panzenboeck).

Author contributions

C.C.G. and U.P. conceived and designed the study. C.C.G, U.P., P.H., D.K., K.K., and A.L. designed experimental approaches. C.C.G., N.M.A., E.F-D., M.Z., Y.S., M.R., V.S., F.R., A.S., A.A., and C.T-A. performed studies, data acquisition, data interpretation, and statistical analysis. C.C.G., U.P., A.L., and K.K. drafted and thoroughly revised the manuscript. All authors revised the manuscript and approved the final version. C.C.G. and U.P. are the guarantors of this work and, as such, had full access to all of the data in the study and take responsibility for the integrity of the data and the accuracy of data analyses.

Declaration of Competing Interest

There are no potential conflicts of interest relevant to this article.

Europe PMC Funders Author Manuscripts

levels in brain. Reduced cerebral and cerebrovascular IR-β and LRP-1 levels in 3XTg-AD mice correlated with elevated levels of autophagy marker LC3B. In both genotypes, high-fat diet (HFD) feeding decreased cerebral and hepatic LRP-1 expression and elevated cerebral Aβ burden without affecting cerebrovascular LRP-1 and IR-β levels. *In vitro* studies using primary porcine (p)BCEC revealed that Aβ peptides 1–40 or 1–42 (240 nM) reduced cellular levels and interaction of LRP-1 and IR-β thereby perturbing insulin-mediated signaling. Further mechanistic investigation revealed that Aβ treatment accelerated the autophagy-lysosomal degradation of IR-β and LRP-1 in pBCEC. LRP-1 silencing in pBCEC decreased IR-β levels through post-translational pathways further deteriorating insulin-mediated responses at the BBB. Our findings indicate that LRP-1 proves important for insulin signaling at the BBB. Cerebral Aβ burden in AD may accelerate LRP-1 and IR-β degradation in BCEC thereby contributing to impaired cerebral and cerebromicrovascular insulin effects.

Keywords

Alzheimer's disease; Amyloid-β peptides; Low-density lipoprotein receptor-related protein-1; Insulin receptor-beta; Insulin signaling; Blood-brain barrier; Endothelial cells; Autophagy-lysosomal pathway

1 Introduction

Insulin receptors (IRs) and their signaling apparatus are widely conserved in various regions of the brain (Kleinridders et al., 2014; Werther et al., 1987). Insulin is known to preserve cognition by conducting crucial neurotrophic functions and by regulating energy metabolism in the brain. Insulin signaling pathways in the CNS, similar as in peripheral tissues, are mediated by the phosphoinositide 3-kinase (PI3-K) and mitogen-activated protein kinase (MAPK) cascades (Zeng et al., 2016). Mounting evidence suggests a crucial link between Alzheimer's disease (AD) and impaired brain insulin signaling (Liu et al., 2011b; Matsuzaki et al., 2010; Mullins et al., 2017). First, epidemiological studies suggest an elevated risk of AD in diabetic patients (Talbot et al., 2012). Second, impaired brain insulin signaling was reported in two different AD mouse models, as well as impaired central and peripheral insulin signaling in young and aged APP_{swe}, PSI_{M146V}, tau_{P301L} (3XTg-AD) mice (Velazquez et al., 2017). Change in cerebral IR levels in human AD is still a matter of debate. For example, diminished IR and insulin like growth factor receptor (IGFR) gene levels were reported in AD *post mortem* brain tissue (Steen et al., 2005), and impaired response to insulin-induced activation of the insulin receptor substrate-1 (IRS-1) signaling pathway was detected in cortex tissue from *post mortem* AD brains (Talbot et al., 2012). In contrast, no such change in human IR protein levels were identified in AD post-mortem brain samples when compared to age matched healthy post-mortem brains, despite that IGFR and IR signaling was compromised in AD neurons suggesting that degenerating neurons in AD may be resistant to IGF-1R/IR signaling (Moloney et al., 2010). Third, high-fat diet (HFD) feeding caused memory deficits in several transgenic mouse models of AD and these deficits coincided with peripheral and central insulin resistance (Knight et al., 2014; Pratchayasakul et al., 2011; Takeda et al., 2010). The 3XTg-AD mice demonstrate elevated brain soluble amyloid beta peptide (Aβ) levels and larger amyloid plaque burden

upon long-term HFD feeding, which was previously shown to increase peripheral insulin resistance, and a single dose of intravenous (i.v.) insulin injection mitigated these effects (Vandal et al., 2014).

The blood-brain barrier (BBB) was assumed to be the main portal for insulin delivery into brain (Pardridge et al., 1985). The IR is expressed at the BBB and high affinity binding sites for insulin were identified on the luminal side of the BBB (Miller et al., 1994). Insulin uptake into brain appears to be facilitated by saturable, receptor-mediated endocytosis in BBB endothelial cells (Frank et al., 1986; Gray et al., 2017; Miller et al., 1994). With increasing age, the cerebral response to peripheral insulin declines in parallel with a reduced cerebrospinal fluid to serum ratio of insulin (Sartorius et al., 2015). Insulin signaling at the BBB is known to regulate cell proliferation and tight-junction integrity (Ito et al., 2017). However, the expression and regulation of IR-β, the major subunit of IR with intrinsic tyrosine kinase activity, and various insulin signaling components at the BBB in AD have not been thoroughly investigated.

Low-density lipoprotein receptor-related protein-1 (LRP-1) is expressed in BBB endothelial cells and represents the major multi-functional scavenging receptor responsible for brain to blood Aβ clearance, as well as Aβ clearance from plasma by the liver (Deane et al., 2004; Ramanathan et al., 2015; Shibata et al., 2000; Tamaki et al., 2006). The intracellular domain of LRP-1 binds to phosphatidy-linositol-binding clathrin assembly protein to regulate endosomal transcytosis of Aβ at the BBB (Ramanathan et al., 2015; Zhao et al., 2015). LRP-1 expression levels are closely associated with lipid and Aβ homeostasis in brain and plasma. Low levels of LRP-1 were reported in AD patient's brain (Kang et al., 2000), cerebrovasculature, and of soluble LRP-1 (sLRP-1) in plasma (Deane et al., 2004; Shibata et al., 2000). Functional knock-out (KO) of LRP-1 in murine brain capillary endothelial cells (mBCEC) from 5xFAD mice induced impaired Aβ clearance from the brain (Storck et al., 2016). Furthermore, Liu et al. reported impaired brain lipid metabolism and progressive age-dependent neurodegeneration in neuronal LRP-1 KO mice (Liu et al., 2010). In accordance with the above, an augmentation of sLRP-1 levels by i.v. infusion was shown to ameliorate brain Aβ pathology in APP +/sw mice (Sagare et al., 2007). Intriguingly, LRP-1 has been identified as a binding partner for IR and to affect insulin signaling upon dimerization with IR-β. LRP-1 knockout in mice reduced IR-β levels and activity, thereby provoking impaired insulin-mediated effects in the brain and in neurons (Fuentealba et al., 2009; Liu et al., 2015).

Given the importance of LRP-1 for Aβ clearance (Storck et al., 2016) and IR-β for insulin responses and/or uptake at the BBB respectively, we aimed to uncover factors and mechanisms regulating LRP-1 and IR-β function in cerebrovascular insulin signaling in AD. For *in vivo* studies, we employed 3XTg-AD mice, carrying mutations for amyloid precursor protein (APP_{swe}), presenilin 1 ($PS1_{M146V}$) and tau_{P301L} (Oddo et al., 2003). We emphasized on establishing the effects of HFD feeding on peripheral, cerebral and cerebromicrovascular LRP-1 and IR-β expression, comparing conditions of early Aβ pathology in 3XTg-AD with non-transgenic (NTg), as well as between male and female mice. Using a well-established *in vitro* primary porcine brain capillary endothelial cell (pBCEC) model, we examined more closely whether and how Aβ modulates insulin-mediated responses and LRP-1/IR-β

homeostasis at the BBB. In addition, an intrinsic link between LRP-1 mediated IR-β regulation and insulin signaling was explored in pBCEC.

2 Material and methods

2.1 Animals and diet

Animal experiments were approved by The Austrian Federal Ministry of Science, Research and Economy (approval number 66.010/130-WF/V/3b/2015). Animals were maintained under standard housing conditions with controlled humidity, temperature, free access to water, and a 12 h light/dark cycle. Male and female 3XTg-AD ($PS1_{M146V}$, APP_{Swe}, and tau_{P301L}) and NTg (C57/BL6) (Zenaro et al., 2015) mice were used for the study. Inbred 3XTg-AD mouse litters were genotyped for human APP_{Swe} and $PS1_{M146V}$ genes after extracting DNA from tail tips; PCR was performed using primers for human APP_{Swe} and $PS1_{M146V}$ provided by The Jackson Laboratories, and mice tested homozygous for both genes were selected for feeding studies (Supplementary Fig. 1). Mice were fed either high-fat/high-cholesterol diet (HFD) containing 60% kcal from fat (D12492, ssniff® diets, Germany) or chow diet containing 12% kcal from fat, for 23 weeks starting from 12 weeks after weaning. Body weights were recorded weekly. Oral glucose tolerance test (OGTT; see2.2.) and Barnes Maze test (BM; see2.3.) were performed after 13 and 20 weeks of feeding, respectively. In female mice the stage of estrus cycle was assessed by vaginal smear analysis (Caligioni, 2009) on the day before sacrifice, which indicated that regardless of the feeding conditions both 3XTg-AD and NTg mice were in transition between metestrus (presence of cornified and nucleated epithelial cells) and anestrus cycle (presence of leucocytes). On day of sacrifice (age: 35 ± 2.7 weeks, referred to as 9-month-old), animals were fasted (6 h) and euthanized under CO_2 flow. Blood was collected by cardiac puncture and plasma was prepared by centrifuging (2000 ×*g*, 15 min). Cerebral microcapillaries were isolated as described under 2.5. Plasma and organs were stored at −80 °C for further analysis. Plasma insulin levels were determined using Ultra-Sensitive Mouse Insulin ELISA Kit (Crystal Chem, USA). Plasma levels of non-esterified fatty acids (NEFA), cholesterol and triglycerides were determined using enzymatic kits provided by DiaSys Diagnostic Systems GmbH, according to the manufacturer's instructions.

2.2 Oral glucose tolerance tests

For OGTT, blood was drawn through the tail vein of mice fasted for 6 h before (0 min) and after 15, 30, 60, 120 min of oral gavage of 2 g of D-glucose/kg body weight. Blood glucose levels were measured immediately using Glucometer Accu-check-active strips (Roche Diagnostics).

2.3 Behavioral tests

Spatial learning and memory was assessed by using the BM test as previously described (Attar et al., 2013; Pitts, 2018). In brief, mice were placed on an elevated round wooden board (diameter: 90 cm) with 20 equally-spaced holes (diameter: 5 cm) at the edge. Mice were habituated to this maze (day 1) and then trained to find a target hole connected to a hidden black escape box (11 × 5 × 5 cm) beneath the maze for 3 days (2 trials/day). The latency to approach the first hole was used to identify any influence on locomotor or

anxiety-like behavior, while the latency to find the target-hole was used to assess learning capabilities. The behavior of the animals during the trials was videotaped and tracked with VideoMot 2 software (TSE Systems, Bad Homburg, Germany).

2.4 Amyloid-β ELISA

Frozen brain cortical hemispheres from male and female 3XTg-AD mice were used to isolate diethylamine (DEA; Sigma-Aldrich) soluble and formic acid (FA; Sigma-Aldrich) soluble Aβ applying the method described by (Casali and Landreth, 2016). In brief, mechanically homogenized brain lysates were mixed with equal volumes of 0.4% DEA solvent (200 μl DEA, 1 ml of 5 M NaCl and 50 ml of ddH_2O) and were centrifuged at 135,000 ×*g* for 1 h at 4 °C, the supernatant was neutralized with 0.5 M Tris-HCl and stored at −80 °C. The resulting pellet was sonicated on ice in 95% FA (~20 s with 15 mA amplitude) until dissolved, and centrifuged at 109,000 ×*g* for 1 h at 4 °C. The supernatant was neutralized with FA neutralization buffer (1 M Tris, 0.5 M Na_2HPO_4 and 0.05% NaN_3) and the samples were stored at −80 °C. Levels of DEA and FA soluble $A\beta_{1–40}$ and $A\beta_{1–42}$ were determined using ELISA kits from ThermoFisher Scientific according to the manufacturer's indications. Quantification was achieved by generating a standard curve using a 4 parameter algorithm to obtain the best fit. Peptide concentrations were normalized to total brain protein content determined by BCA assay (pg/mg wet weight).

2.5 Isolation of murine brain microvessels

Brains were harvested and microvessels were isolated from 3 to 4 pooled brain hemispheres (Zandl-Lang et al., 2018). In brief, brain hemispheres devoid of meninges and olfactory bulbs were homogenized in MCDB131 medium (containing 2% FBS, 1% L-glutamine and 1% penicillin/streptomycin), subjected to dispase digestion (0.01 g/2 hemispheres, 1 h, 37 °C; Life Technologies), followed by a centrifugation step (6800 ×*g*) using dextran solution (1:1 v/v, 1.0612 g/L; Alfa Aesar), and followed by a brief collagenase/dispase (3.5 mg/20 ml, 1 min, 37 °C; Roche) digestion to detach the basement membrane from the endothelium, filtering the suspension through a nylon mesh (180 μm), and purification of microcapillary fragments after centrifugation in a Percoll (Sigma-Aldrich) density gradient from which mBCEC were collected from the interface. Rinsed cell pellets were stored at −80 °C for further analyses. Purity of isolated cerebromicrovascular fragments/mBCEC was assessed by both transcriptional and immune-fluorescent detection of cell-specific marker genes/proteins (Supplementary Figs. 3 & 4).

2.6 Isolation of porcine brain capillary endothelial cells (pBCEC)

Primary pBCEC were isolated from brains of young, adult pigs (Chirackal Manavalan et al., 2014). In brief, three hemispheres were cleared of meninges using forceps and were minced using a cutter with rolling blades. Minced brain tissue was enzymatically homogenized by gentle stirring in a water bath for 1.5 h at 37 °C in preparation medium (M199 containing 1% penicillin/streptomycin, 1% gentamycin and 1 mM L-glutamine) containing dispase (Life Technologies; 70 mg/150 ml;). After homogenization, dextran solution (1:1 v/v, 1.0612 g/L; Alfa Aesar) was added and the suspension was centrifuged at 6800 ×*g* for 10 min at 4 °C to separate myelin from the vessel pellet. Resuspened vessel pellets were strained through a nylon mesh (180 μm pore size) to purify microvessels. Homogenate containing

microvessels was briefly incubated with collagenase/dispase (3.5 mg/20 ml) for 1 min at 37 °C to disrupt basement membranes, followed by purification of cerebromicrovascular fragments/BCEC using a biphase percoll gradient (20 ml of 1.03 g/ml percoll solution underlaid with 15 ml 1.07 g/ml percoll solution) and centrifuging at 1300 ×*g* for 10 min at room temperature (RT). BCEC collected at the percoll biphase gradient interface were washed and cultured in collagen coated 75 cm^2 flasks supplemented with M199 medium (1% penicillin/streptomycin, 1 mM L-glutamine, 10% horse serum, 95% humidity, 5% CO_2). After reaching 80–90% confluency, cells were trypsinized and seeded onto 6- or 12-well plates or chamber slides (Lab-Tek) for further experiments.

2.7 Preparation of insulin and Aβ peptides for *in vitro* experiments

Human recombinant insulin (Calbiochem®, Merck) was dissolved in 0.01 N hydrochloric acid (HCl) to obtain a 10 mM stock solution, stored at 4 °C, and used within 4 weeks according to manufacturer's instructions (Chirackal Manavalan et al., 2014). Amyloid beta peptides ($A\beta_{1–40}$ and $A\beta_{1–42}$) were prepared according to manufacturer's instructions (rPeptide, Watkinsville, GA, USA). In brief, hexafluoro-2-propanol (HFIP) treated $A\beta_{1–40}$ and $A\beta_{1–42}$ films were dissolved in 1% ammonium hydroxide (Sigma-Aldrich) to obtain a concentration of 1 mg/ml. Then, solutions were briefly vortexed and sonicated in a water bath for 30 s until they were clear and free from aggregates. Aβ preparations were frozen in aliquots at −80 °C. On day of use, fresh $A\beta_{1–40}$ and $A\beta_{1–42}$ aliquots were brought to room temperature and were immediately used. Aggregation profiles of $A\beta_{1–40}$ and $A\beta_{1–42}$ peptides are shown in the Supplementary Fig. 2. For all *in vitro* experiments in pBCEC, 240 nM (1 μg/ml) of $A\beta_{1–40}$ and $A\beta_{1–42}$ peptides were used.

2.8 SDS-PAGE and immune-blotting (IB)

Brain cortical tissue, liver, mBCEC, or pBCEC were lysed by brief sonication in protein lysis buffer (containing 50 mM Tris, 10 mM EDTA, 1% Triton X 100, phosphatase inhibitor (PhosSTOP™), protease inhibitor cocktail (Roche Diagnostics cOmplete™), and pH adjusted to 7.5). Protein quantification was performed using bicinchoninic acid assay (BCA, ThermoFisher Scientific). Samples were mixed (4:1) with XT loading buffer (Bio-Rad) and proteins were denatured at 90 °C for 5 min. Proteins (20 μg/well) were loaded on NuPage® Novex 4–12% Bis-Tris Midi gels and separated under reducing conditions by SDS-PAGE using 1× MOPS or MES (Life Technologies) buffer. Then, proteins were electroblotted onto 0.45 μm polyvinylidene difluoride membranes (PVDF; GE Healthcare). Membranes were blocked with 5% non-fat dry milk protein (Bio-Rad) for 1 h at room temperature (RT). Membranes were incubated with primary antibody overnight in 5% bovine serum albumin (BSA; Roche) at 4 °C, followed by HRP-conjugated secondary antibody incubation in 5% non-fat dry milk protein for 1 h at RT. Detection of immune-reactive bands was performed using Clarity Western ECL Substrate (Biorad) and a ChemiDoc imager (Bio-Rad). Band intensities were determined using ImageLab software (version 5.2.1, Bio-Rad). All primary and secondary antibodies used are listed in Supplementary Table 1.

2.9 Immune-fluorescent staining (IF)

For immune-cytochemistry (Zandl-Lang et al., 2018), pBCEC were cultured on Lab-Tek chamber slides (Thermo Fisher Scientific, NY, USA). Cells were fixed with acetone and air

dried. Mouse brain immune-fluorescent (IF) stainings were carried out on 18 μm cryosections of cortex and fixed with 4% paraformaldehyde (PFA). Cells or sections were rinsed and blocked with donkey serum prior to primary antibody incubation for 1 h. Negative controls were incubated with the appropriate IgG fractions as isotope controls. After TBST wash, secondary antibodies were applied. DAPI was used as a nuclei counter stain. Sections were rinsed with TBST before mounting with Vectashield mounting medium (Vector Lab, Inc., Burlingame, CA, USA). To acquire and analyze computerized images of sections and cells, a Leica DM4000 B microscope (Leica Cambridge Ltd.) equipped with Leica DFC 320 Video camera (Leica Cambridge Ltd.) was used. Antibodies used for the IF stainings are listed in Supplementary table 2.

2.10 LRP-1 and IR-β silencing in pBCEC

Three targeting siRNAs for each target gene, *i.e.* porcine LRP-1 (5′-GGAGGAUGACUGUGAACAU-3′, 5′-ACAACGCUGUCGCCUUGGA-3′ and 5′-CCUGUACUGGUGUGACAAA-3′) and porcine IR-β (5′-GGGUCCGGAUAUAAAUUAA-3′, 5′-GAAAUGGAGUGCAUGUAAA-3′ and 5′-ACACAGGCUUUGAUAUAGA-3′), were purchased from Microsynth. Non-targeting control (NTC) siRNAs were purchased from Dharmacon Research. Primary pBCEC at 70–90% confluency were transfected with DharmaFECT transfection reagent (Dharmacon) following manufacturer's instructions and as described in (Kober et al., 2017). In brief, three siRNAs for each target gene (LRP-1 or IR-β) were pooled in nuclease free water to attain 5 μM stock solutions. For silencing experiments, cells were cultured in 6-well plates and incubated with pooled LRP-1/IR-β/NTC siRNAs (50 nM) along with DharmaFECT transfection reagent (10 μl/well) in serum free (SF) medium according to the manufacturer's instructions. After 24 h of incubation, medium was replaced with M199, containing 5% horse serum for 24 h. Cells were harvested at indicated time points and silencing efficiency was determined using qRT-PCR (2.11.) and IB. For insulin treatments, after 48 h silencing, cells were serum starved for 12 h in SF medium prior to insulin stimulation.

2.11 RNA isolation and quantitative real-time PCR (qRT-PCR)

Total cellular RNA was isolated using TriReagent RT (MRC, USA). Complementary DNA was prepared using High Capacity Reverse Transcriptase Kit (Life Technologies) following the manufacturer's guidelines. Quantitative real-time PCR (qRT-PCR) was performed using SYBR Green Master Mix (Biorad) on a CFX96 Real time system (Biorad). Relative gene expression was quantified using the $2^{-\Delta\Delta Ct}$ method after normalizing the target gene expression with reference gene hypoxanthine phosphoribosyltransferase 1 (HPRT-1) (Kober et al., 2017; Zandl-Lang et al., 2018). Primer pairs used are listed in the Supplementary Table 3.

2.12 Quantification of LC3B dot coverage of cerebrovascular endothelial cells

Image data was acquired using the method previously described by Yang and colleagues (Yang et al., 2003). In brief, from each double immune-fluorescent image of 18 μM mouse brain cryosections stained for microtubule-associated protein 1A/1B light chain 3B (LC3B) and platelet endothelial cell adhesion molecule (PECAM/CD31), three 1 mm^2 fields were

randomly chosen and LC3B dots on CD31 coverage area were counted. Image acquisition and digital image quantification were performed using NIH Image J software.

2.13 Statistical analysis

Two-tailed Student's unpaired *t*-test, one-way ANOVA followed by Dunnett's multiple comparisons test, or two-way ANOVA analysis were used to analyze differences between groups (GraphPad Software, Inc., La Jolla, CA). $p < 0.05$ was considered statistically significant. All data are presented as means ± SD, N referring to the number of mice in each group; n referring to the number of independent *in vitro* experiments with different pBCEC isolations performed. For BM test, statistical data analysis was performed on SPSS 24 (IBM SPSS Statistics, Vienna, Austria) and SigmaPlot 13 (Systat Software Inc., San Jose, CA, USA). Between and within subject differences were assessed by two-way repeated-measures ANOVA. Post-hoc analysis of group differences was performed by one-way repeated measures ANOVA or by two-way ANOVA followed by Tukey's *post hoc* comparison, as appropriate. Probability values < 0.05 were regarded as statistically significant. BM data are presented as mean ± SEM, N referring to the number of mice in each group.

3 Results

3.1 Plasma insulin and lipid profiles in chow *vs* HFD fed male and female 3XTg-AD and NTg mice

Male and female 3XTg-AD and NTg mice were fed with standard chow or HFD for 23 weeks. OGTT was performed after week thirteen, to assess the impact of HFD on peripheral glucose tolerance and insulin sensitivity. As expected, HFD feeding for 23 weeks induced significant body weight gain in both genders and genotypes (Fig. 1A), which was accompanied by decreased glucose tolerance (OGTT; Fig. 1B). ANOVA indicated that HFD feeding significantly enhanced body weight (BW) gain in NTg mice (male: $F_{20,377} = 20.13$, $p < 0.0001$ and female: $F_{20,355} = 1.78$, $p < 0.0221$) and in 3XTg-AD mice (male: $F_{20,245} = 3.15$, $p < 0.0001$ and female: $F_{20,261} = 3.92$, $p < 0.0001$) *vs* chow fed mice. Moreover, female 3XTg-AD mice showed a higher food intake resulting in higher BW gain (87 ± 20.1% *vs* chow fed 3XTg-AD mice; $F_{20,261} = 3.92$, $p < 0.0001$) than female NTg mice (39 ± 7.7% *vs* NTg chow fed mice; $F_{20,355} = 1.77$, $p < 0.022$). Interestingly, food intake in HFD fed male 3XTg-AD mice and NTg female mice was significantly lower ($p < 0.001$) compared to HFD fed counterparts (Fig. 1C). In correspondence to BW gain, HFD feeding impaired glucose tolerance in both NTg (male: $F_{5,102} = 8.02$, $p < 0.0001$ and female: $F_{5,108} = 6.55$, $p < 0.0001$) and 3XTg-AD (male: $F_{5,65} = 3.287$, $p < 0.05$ and female: $F_{5,84} = 3.92$, $p < 0.0001$) mice *vs* chow fed mice. Interaction between sexes was observed in NTg and 3XTg-AD mice. HFD fed NTg female mice showed better glucose tolerance when compared to HFD fed NTg male mice ($F_{5,108} = 2.62$, $p < 0.0282$), corresponding to food intake and body weight gain. However, chow fed 3XTg-AD female mice showed better glucose tolerance when compared to male 3XTg-AD mice ($F_{5,72} = 4.36$, $p < 0.0016$). Interaction between 'transgene' (*i.e.* genetic differences) was observed in chow and HFD fed, NTg and 3XTg-AD male mice, NTg chow (M) *vs* 3XTg-AD chow (M) ($F_{5,78} = 3.59$, $p < 0.0057$) and NTg HFD (M) *vs* 3XTg-AD HFD (M) ($F_{5,102} = 4.05$, $p < 0.0021$). Low but not significantly different ($p = 0.051$) fasting plasma insulin levels (Fig. 1D) were detected in

male 3XTg-AD *vs* NTg mice. Female NTg and 3XTg-AD mice showed significantly lower fasting plasma insulin levels when compared to their male NTg and 3XTg-AD counterparts. In NTg mice, HFD feeding significantly elevated plasma insulin levels by 326 ± 181.2% in male and 114 ± 62.2% in female mice. Interestingly, no significant increase in insulin levels was observed in HFD fed 3XTg-AD mice (Fig. 1D). Significantly elevated NEFA (65 ± 9.2%), triglycerides (30 ± 6.5%) and cholesterol (62 ± 21.5%) levels were detected in female 3XTg-AD as compared to female NTg mice (Fig. 1E–G). While elevated plasma NEFA levels and triglycerides (3XTg-AD HFD (M) mice) were detected in both male and female 3XTg-AD mice independent of HFD feeding (Fig. 1E), no differences in plasma triglycerides and cholesterol were observed in male mice of either genotype (Fig. 1F&G).

3.2 Impact of gender and diet on cerebral Aβ burden and memory in 3XTg-AD mice

Since HFD feeding is known to aggravate brain Aβ pathology in older (15 months) female 3XTg-AD mice (Vandal et al., 2014), by using ELISA we quantified soluble (*i.e.* DEA extracted oligomeric and prefibrillary Aβ) and insoluble (*i.e.* FA extracted fibrillary Aβ aggregates) $A\beta_{1–40}$ and $A\beta_{1–42}$ in brain homogenates of our 9-month-old male and female, chow- and HFD-fed 3XTg-AD mice. $A\beta_{1–40}$ and $A\beta_{1–42}$ was not detectable in NTg mouse brain lysates (not shown). Overall, female 3XTg-AD mice revealed by 2.7 ± 0.83 and 5.2 ± 0.12-fold higher soluble and 4.8 ± 0.33 and 4.1 ± 0.14-fold higher insoluble $A\beta_{1–40}$ and $A\beta_{1–42}$ levels when compared to male mice (Fig. 2A&B). When on HFD, soluble $A\beta_{1–40}$ levels were significantly higher in female HFD-fed 3XTg-AD mice (57 ± 10.0%) *vs* chow fed 3XTg-AD mice, but below detection limit in male mice. Male and female HFD-fed 3XTg-AD mice exhibited significantly higher soluble $A\beta_{1–42}$ levels (males: 62 ± 9.1% and females: 91 ± 7.2%) *vs* chow fed 3XTg-AD mice (Fig. 2A). However, no significant changes were observed in insoluble $A\beta_{1–40}$ and $A\beta_{1–42}$ levels (Fig. 2B). In addition, Aβ targeted IF staining (using 6E10 antibody) of hippocampal cryosections revealed staining of Aβ plaques in brains of both chow and HFD fed male and female 9-month-old 3XTg-AD mice, whereas only faint staining was observed in NTg mice (Fig. 2C).

Since HFD was further reported to impair memory in old, female 3XTg-AD mice (Knight et al., 2014; Vandal et al., 2014), we also tested whether HFD feeding in 9-month-old male and female 3XTg-AD and NTg mice has effects on memory and anxiety behavior. Interestingly, BM analysis revealed significant behavioral changes reflecting anxiety and memory in female, but not in male 3XTg-AD mice. The latency to find the target hole revealed that the learning performance of female mice over multiple trials correlated with both the genotype and the diet (Fig. 2D): female 3XTg-AD mice on chow or HFD feeding showed impaired target hole latency ($F_{1,27} = 20.161$; $p < 0.001$ and $F_{1,27} = 6.308$; $p = 0.018$ *vs* respective chow and HFD fed NTg controls) (Fig. 2D); first-hole latency time, a parameter to determine anxiety, worsened upon HFD feeding in female 3XTg-AD mice ($F_{1,27} = 8.166$; $p = 0.008$ *vs* NTg controls) (Fig. 2E). However, no such differences in anxiety and/or memory were observed in male 3XTg-AD mice of both feeding regimens (Fig. 2F&G).

3.3 The 3XTg-AD transgene and HFD feeding affect liver LRP-1 and IR-β expression

Since insulin mediates LRP-1 regulation and plays a crucial role also in peripheral Aβ clearance (Tamaki et al., 2006; Tamaki et al., 2007), we first explored if IR-β and LRP-1

expression are modulated in peripheral tissue. Therefore, we subjected liver lysates of 3XTg-AD and NTg mice to IB and determined LRP-1, IR-β, and pAKT/AKT protein levels. Liver IR-β levels were moderately but significantly down-regulated by 26 ± 4.5% in male and 25 ± 4.0% in female chow fed 3XTg-AD mice as compared to NTg mice (Fig. 3A&B). Similarly, feeding NTg mice a HFD led to decreased IR-β levels by 22 ± 1.3% when compared to chow fed male but not female mice (Fig. 3A&B). Lower hepatic IR-β levels in 3XTg-AD mice maintained on either feeding regimens coincided with lower circulating insulin levels, which is indicative of hepatic insulin resistance. Interestingly however, chow fed 3XTg-AD mice did not show altered hepatic LRP-1 levels (Fig. 2C), but HFD feeding significantly decreased hepatic LRP-1 levels by 54 ± 21.0% and 49 ± 18.9% in both NTg and 3XTg-AD males compared to the corresponding chow diet controls (Fig. 3A&C). The pAKT levels in liver lysates were significantly elevated by 105 ± 22.5% in males and 106 ± 32.2% in females 3XTg-AD chow fed mice compared to NTg mice (Fig. 3A&D). However, HFD feeding significantly decreased hepatic pAKT levels in male and female 3XTg-AD mice (Fig. 3A&D). In contrast, HFD feeding led to increased hepatic pAKT levels in male NTg mice ($p < 0.05$), which was not evident in female NTg mice. Together, these results indicate that 3XTg-AD mice exhibited impaired hepatic IR-β levels and hyper-activated downstream AKT levels; HFD feeding exerted a modest effect on hepatic IR-β levels in these mice. In contrast, HFD feeding clearly induced downregulation of LRP-1 levels in livers of both genotypes.

3.4 Cerebral IR-β/LRP-1 homeostasis and insulin signaling is impaired in 3XTg-AD mice

We next analyzed the effect of HFD feeding on IR-β/LRP-1 homeostasis and insulin signaling in the brain (Fig. 4A&B). 3XTg-AD mice exhibited marked reductions in brain IR-β protein levels by 49 ± 13.7% in males and 35 ± 6.6% in females compared to NTg mice (Fig. 4A&C). HFD feeding further decreased cerebral IR-β levels by 30 ± 5.4% in 3XTg-AD female mice but not in male mice compared to their chow fed counterparts (Fig. 4C). The general pattern of lower IR-β levels in brain lysates of 3XTg-AD *vs* NTg mice was also evident (Fig. 4C). Moreover, a reduction in pIRS-1 (S1101) levels was detected in brain lysates of male 3XTg-AD mice by 37 ± 7.5% and female mice by 47 ± 25.8% compared to chow fed NTg mice (Fig. 4E). However, HFD feeding did not lead to decreased IRS-1 phosphorylation in brain, irrespective of genotype or gender; on the contrary, female NTg mice on HFD exhibited increased pIRS-1 levels, $p < 0.001$ *vs* chow fed NTg mice (Fig. 4E). Furthermore, chow fed 3XTg-AD mice exhibited increased phosphorylation of cerebral AKT and ERK as compared to NTg mice of same gender (Fig. 4F&G). HFD feeding decreased cerebral pAKT but not pERK levels in 3XTg-AD mice (Fig. 4F&G). In contrast, HFD feeding of NTg mice did not affect cerebral pAKT or pERK levels in male mice but led to increased pERK levels in female mice (Fig. 4F&G). Interestingly, a significant reduction in LRP-1 protein levels by 57 ± 34.4% in the brain lysates of male and 46 ± 21.9% in female 3XTg-AD mice was observed as compared to chow fed NTg animals (Fig. 4D), which was paralleled with reduced brain IR-β levels. HFD feeding decreased LRP-1 expression in brains of NTg mice of both genders (by 46 ± 6.9% & 28 ± 1.2% in male and female mice, respectively) as compared to chow fed NTg mice, but not in that of 3XTg-AD mice (Fig. 4B).

3.5 IR-β/LRP-1 homeostasis is dysregulated in cerebromicrovascular endothelial cells in 3XTg-AD mice

Since insulin mediates LRP-1 trafficking in cerebrovascular endothelial cells (Swaminathan, 2017), and LRP-1 is known to regulate Aβ clearance from the brain *via* the cerebrovasculature (Storck et al., 2016), we next investigated whether LRP-1 as well as IR-β levels were altered at the level of the BBB in 3XTg-AD mice. In order to prove the identity of microvascular cells isolated from mouse brains, we performed gene and protein expression analysis of specific markers for endothelial cells, pericytes, astrocytes, and microglia by qRT-PCR (Supplementary Fig. 3) and IF staining, respectively (Fig. 5Aa & Supplementary Fig. 4). Quantitative RT-PCR analyses revealed that cerebromicrovascular CD31 mRNA levels were 31.2 fold higher as compared to whole brain CD31 mRNA levels, confirming a highly enriched endothelial cell fraction is obtained (Supplementary Fig. 3). Messenger RNA expression of pericyte markers aminopeptidase N (APN = CD13) and platelet-derived growth factor receptor beta (PDGFR-β) was low but detectable (Supplementary Fig. 3). Double IF staining of purified cerebral microvessels for IR-β and LRP-1 proteins confirmed the expression of both proteins (Fig. 5Aa&b) in mouse brain microvascular endothelial cells (CD31, red). Furthermore, we identified the expression and co-localization (white) of IR-β (magenta) and LRP-1 (green) in mBCEC of isolated cerebral microvessels (Fig. 5Ac). Protein lysates of purified mBCEC from 3XTg-AD and NTg mice were subjected to IB. Murine BCEC obtained from 3XTg-AD mice exhibited significantly lower LRP-1 expression levels (by 49 ± 6.3% in males and 50 ± 6.7% in females) as compared to NTg mice (Fig. 5B&C). The IR-β expression trends closely paralleled that of LRP-1 expression in 3XTg-AD and in NTg mice; cerebrovascular IR-β was decreased by 41 ± 9.4% in male 3XTg-AD mice and 40 ± 13.5% in female mice when compared to chow fed NTg mice (Fig. 5B&D). As opposed to brain LRP-1 levels, the HFD mediated effects on LRP-1 levels in microvessels purified from male or female 3XTg-AD mice were not very pronounced when compared to chow fed 3XTg-AD mice (Fig. 5C&D).

3.6 Elevated brain and cerebrovascular autophagy in 3XTg-AD mice

Since 3XTg-AD mice showed elevated brain Aβ peptide levels, we were interested to know the status of autophagy and its correlation with impaired LRP-1 and IR-β levels at the cerebrovascular level. Double immune-fluorescent images of CD31 and LC3B staining revealed that LC3B dot coverage in cerebrovascular endothelial cells was significantly higher in both male and female 3XTg-AD mice (190 ± 36% and 266 ± 43%) *vs* respective chow fed NTg mice (Fig. 6A–C). HFD feeding further elevated LC3B dot coverage in cerebrovascular endothelial cells identified in cortical crysections obtained from 3XTg-AD (31 ± 8% and 28 ± 6% from male and female HFD fed 3XTg-AD mice *vs* chow fed 3XTg-AD mice) but not from NTg mice (Fig. 6A–C). In whole brain lysates, 3XTg-AD mice (independent of gender) showed elevated LC3B-II levels demonstrating active autophagy (92 ± 16% and 81 ± 14% in male and female 3XTg-AD mice *vs* respective NTg mice; Fig. 6D). Feeding the HFD elevated brain LC3B-II levels significantly in both genotypes and genders (73 ± 15% and 62 ± 7% in male and female HFD fed NTg mice *vs* respective chow fed NTg mice; 167 ± 37% and 212 ± 41% in male and female HFD fed 3XTg-AD mice *vs* respective chow fed NTg mice) (Fig. 6D&E). Elevated LC3B levels in brain cortex and

cerebral vessels in 3XTg-AD mice correlated with changes in brain Aβ burden (Fig. 2A&B) and changes in LRP-1 and IR-β receptor levels (Fig. 5B–D).

3.7 Aβ treatment disrupts insulin induced LRP-1 expression, IR-β levels, and insulin signaling in an in vitro model of the BBB

Since cerebrovascular LRP-1 and IR-β levels were downregulated in 3XTg-AD mice, effects of Aβ peptides on BBB endothelial LRP-1 and IR-β receptors were explored. Incubation of cultured pBCEC with $A\beta_{1–40}$ or $A\beta_{1–42}$ significantly downregulated insulin induced upregulation in LRP-1 levels by 76 ± 28.3% and 75 ± 32.6%, respectively, as compared to insulin treated pBCEC, which is evident from immune-blots (Fig. 7A). $A\beta_{1–40}$ or $A\beta_{1–42}$ treatment alone induced significant down-regulation of LRP-1 levels by 44 ± 14.8 and 61 ± 16.4, respectively. In parallel, a significant downregulation in IR-β protein levels by 43 ± 13.3% and 50 ± 11.6%, respectively, when compared to vehicle treatment was detected. Enhanced LC3B-I levels were observed upon Aβ incubation, as indicated in immune-blots and quantifications (Fig. 7A&B), indicating autophagy induction. In line with the IB results, double IF stainings for IR-β and LRP-1 revealed reduced receptor expression and co-localization upon $A\beta_{1–40}$ treatment of pBCEC (Fig. 7C). Since both Aβ isoforms clearly affected IR-β levels in pBCEC, we further examined their effects on insulin-mediated signaling by investigating pAKT and pERK protein levels. As expected, we found that insulin treatment of pBCEC increased AKT(S473) phosphorylation by 461 ± 35.2% *vs* vehicle treatment (Fig. 7D&E). In sharp contrast, $A\beta_{1–40}$ or $A\beta_{1–42}$ treatment of pBCEC in the presence of insulin markedly reduced AKT phosphorylation by 67 ± 8.5% and 85 ± 21.8%, respectively, as compared to insulin treated pBCEC (Fig. 7D&E). Incubation of pBCEC with insulin also increased ERK (42/44) phosphorylation by 114.5 ± 18.4% as compared to vehicle treatment (Fig. 7D&F). However, incubation of pBCEC with either $A\beta_{1–40}$ or $A\beta_{1–42}$ alone (in the absence of insulin) led to similarly increased ERK phosphorylation by 121 ± 21.1% and 151 ± 56.6%, respectively, as compared to vehicle treated pBCEC (Fig. 7D&F).

3.8 Aβ induces autophagy-lysosomal degradation of LRP-1 and IR-β in pBCEC

Since cell surface receptor recycling and misfolded protein degradation is controlled by cell autophagy-lysosomal degradation pathway in cooperation with ubiquitin-proteasomal pathway (Kocaturk and Gozuacik, 2018; Lilienbaum, 2013), we next invested whether these pathways are modulated by Aβ peptides in pBCEC. Lysosomal induction was observed in pBCEC upon $A\beta_{1–40}$ treatment, as indicated by enhanced lysosomal-associated membrane protein 1 (LAMP-1) levels in $A\beta_{1–40}$ treaded cells (Fig. 8A,a–d). LRP-1 and IR-β trafficking to lysosomes (LAMP-1, red) was observed, as indicated by co-localization of LAMP-1 (red) with IR-β (green) or LRP-1 (green) in $A\beta_{1–40}$ treated cells (Fig. 8A,c&d). We next studied effects of Aβ treatment on autophagy-lysosomal induction by using specific markers for lysosomal induction (LAMP-1) and autophagy such as LC3B, autophagy-related protein 3 (ATG3) and autophagy-related protein 5 (ATG5). A significant upregulation of LAMP-1 levels by 102 ± 10.4% as compared to vehicle control was identified in Aβ treated cells (Fig. 8A,B&D), which correlated with increased ATG5 (by 87 ± 5.6%) and ATG3 (by 56 ± 15.1%) levels, as compared to vehicle treatment, and significantly reduced LRP-1 and IR-β protein levels, by 59 ± 18.6% and 58 ± 10.6%, respectively, *vs* vehicle treated pBCEC

cells (Fig. 8A,B&D). Treatment with lysosomal inhibitor (chloroquine) rescued Aβ mediated lysosomal degradation of LRP-1 and IR-β proteins. Proteasome inhibition with MG132 partially rescued LRP-1 and IR-β proteins. Both occured predominantly by blocking Aβ mediated lysosomal induction, as depicted by significantly reduced LAMP1 levels upon treatment with Aβ together with chloroquine (by 75 ± 31.5% *vs* $A\beta_{1–40}$ treatment) or MG132 (by 57 ± 19.0% *vs* $A\beta_{1–40}$ treatment) (Fig. 8A,B&D; B,e–l). Chloroquine treatment significantly impaired autophagy-lysosomal degradation in pBCEC, represented by LC3B accumulation as indicated by IB (Fig. 8A,B&D) and IF staining (Fig. 8B,m–p), reduced ATG3 and ATG5 protein levels (Fig. 8A,C&D). In addition, chloroquine treatment significantly reduced proteasomal regulatory proteins, 26S proteasome non-ATPase regulatory subunit 4 (PSMD4), and heat shock protein 27 (HSP27). These findings together indicate that by inhibiting Aβ induced autophagy-lysosomal activity, LRP-1 and IR-β degradation is rescued in pBCEC.

3.9 LRP-1 is important for post-translational regulation of IR-β and insulin signaling in pBCEC

Having established the effects of Aβ treatment on IR-β and LRP-1 expression and their interaction in pBCEC, we next assessed a possible crosstalk between LRP-1 and IR-β that might cause these effects. Therefore, pBCEC were transfected with either LRP-1, IR-β, or mock (non-targeting control, NTC) silencing (si)RNAs. Gene silencing efficiency was confirmed by diminished mRNA expression levels of LRP-1 (47 ± 7.4%) and IR-β (53 ± 12.7%) using qRT-PCR (Fig. 9A&B). The amount of IR-β transcript remained unaltered when LRP-1 was silenced and *vice versa* (Fig. 9A&B), indicating that no crosstalk between IR-β and LRP-1 occured at the mRNA level. However, LRP-1 silencing markedly reduced the protein levels of IR-β by 60 ± 9.2% *vs* NTC siRNA treated pBCEC, independently of insulin treatment of pBCEC (Fig. 9C&D). Similarly, insulin-mediated phosphorylation of IR-β (Tyr1131) and AKT (S473) was hampered by 80 ± 7.2% and 90 ± 7.5%, respectively, upon LRP-1 silencing in pBCEC (Fig. 9F&G). In contrast, silencing of IR-β exhibited no effect on LRP-1 protein levels, while it decreased insulin-mediated phosphorylation of IR-β (Tyr1131) and AKT (S473) in pBCEC by 88 ± 4.2% and 91 ± 5.9% *vs* insulin treated control cells (Fig. 9F&G), independent of changes in LRP-1. In summary, these results suggest that LRP-1 is associated with IR-β receptor expression in BBB endothelial cells and loss in LRP-1 leads to impaired IR-β levels, which in turn affects insulin signaling in pBCEC.

4 Discussion

Aberrant brain insulin signaling is a known hallmark of AD individuals (Bedse et al., 2015; Frolich et al., 1998; Frolich et al., 1999; Matsuzaki et al., 2010), and LRP-1 has been demonstrated recently to regulate neuronal IR-β expression and modulate insulin signaling in the brain (Fuentealba et al., 2009; Liu et al., 2015). Less is known about the interplay and regulation of IR-β and LRP-1 at the BBB and how it is influenced in/by AD. This study employed the 3XTg-AD mouse model and an *in vitro* brain capillary endothelial cell (pBCEC) BBB model to further understand dysregulated insulin signaling in early AD pathology, with a specific focus on LRP-1 and IR-β function in cerebromicrovascular insulin

signaling. Together, our results suggest that Aβ production in the 3XTg-AD model and when added *in vitro* to pBCEC, reduces LRP-1 and IR-β levels by elevating endothelial autophagy-lysosomal induction. Using RNA interference approach, we propose a mechanism whereby reduced LRP-1 in turn decreases IR-β in BCEC thereby reducing insulin mediated response at the BBB.

Fasting plasma insulin levels were higher in male mice, independent of diet. HFD feeding led to elevated plasma insulin levels only in NTg but not in 3XTg-AD mice (Fig. 1D) which is in line with previous findings (Griffith et al., 2019; Vandal et al., 2015; Vandal et al., 2014). In our studies, 3XTg-AD mice showed elevated plasma lipid levels, including NEFA, TG, and cholesterol (Fig. 1D–G). These elevated lipids may infer to a change in metabolic profile due to the transgenes and/or Aβ pathology and/or diet-mediated effects. The effect of HFD feeding was more prominent in female mice, which are prone to a more aggressive AD phenotype than their male counterparts (Carroll et al., 2010). This was reflected by elevated brain soluble and insoluble levels of Aβ detected in female compared to male 3XTg-AD mice (Fig. 2A–C). Our findings support previously reported gender differences in Aβ pathology observed in 3XTg-AD mice (Carroll et al., 2010; Clinton et al., 2007; Hirata-Fukae et al., 2008). During BM analysis, female 3XTg-AD mice displayed disturbed memory, which was further aggravated by HFD feeding (Fig. 2F&G), whereas male 3XTg-AD mice (of both feeding regimens) showed no disturbance in memory or anxiety behavior (Fig. 2D&E).

Of note, Aβ forms deposits also in pancreatic islets in female 3XTg-AD mice (Vandal et al., 2014), which is paralleled by impaired insulin production *via* apoptotic caspase-3 induction and pancreatic islet degeneration, exacerbated upon HFD feeding, and can be rescued by insulin (Griffith et al., 2019; Vandal et al., 2015; Vandal et al., 2014). We observed altered lipid profiles in 3XTg-AD mice that are likely associated with diminished IR-β levels detected in liver (Fig. 3B), brain (Fig. 4C), and at the BBB (Fig. 5). Diminished IR-β levels detected in liver and brain homogenates of 3XTg-AD mice directly affected hepatic and cerebral insulin signaling as evident by reduced serine phosphorylation of IRS-1 (Fig. 4E), followed by a hyperactivation of downstream insulin signaling molecules like AKT (Fig. 4F), mTOR (Caccamo et al., 2010), and ERK (Fig. 4G). Hyperactivation of downstream insulin signaling in 3XTg-AD mice was proposed to associate with “selective insulin resistance”, (Kucejova et al., 2016; Velazquez et al., 2017), a paradoxical downstream insulin signaling activation state that may disrupt upstream insulin signaling by downregulating the phosphorylation of upstream mediators like IR and receptor associated proteins. Such negative feed-back mechanism however does not fully explain the present findings, particularly given that ERK signaling in 3XTg-AD mice and AKT signaling in HFD-fed mice were affected as predicted, *i.e.* decreased pAKT and elevated ERK levels (Fig. 4F&G). Even though ERK is activated in response to insulin and has a positive effect on cell growth, it also participates in insulin signaling malfunction and its inhibition can prevent TNFα-induced insulin resistance (Engelman et al., 2000; Ghasemi et al., 2014; Subramaniam and Unsicker, 2010). Similarly, IR-β silencing in pBCEC resulted in decreased AKT signaling. (Fig. 9C&G). However, increased AKT activity along with decreased IR-β levels (at the BBB) in 3XTg-AD mice is in good agreement with another working hypothesis for how diabetes modifies AD risk suggesting that reduced (central)

insulin signaling in diabetes results in GSK3B activation, tau hyperphosphorylation, and NFT formation (Jolivalt et al., 2008; Steen et al., 2005; Yang et al., 2013).

Diminished IR-β levels in brain and at the BBB coincided with changes in LRP-1 levels in 3XTg-AD mice (Fig. 5B–C). Insulin was shown to elevate neuronal LRP-1 levels (Liu et al., 2015) and is known to promote surface mobilization of LRP-1, thus improving LRP-1 mediated Aβ clearance in hepatocytes (Tamaki et al., 2007) and also at the BBB (Swaminathan, 2017). As previously reported, LRP-1 has the ability to mediate insulin signaling by dimerizing with IR-β; knocking out LRP-1 adversely affects insulin-mediated responses in neuronal cells (Fuentealba et al., 2009; Liu et al., 2015). Moreover, reduced brain and cerebrovascular LRP-1 levels were reported in human subjects with AD (Deane et al., 2004; Kang et al., 2000; Shibata et al., 2000).

Our results of decreased brain LRP-1 (Fig. 4D) and IR-β levels (Fig. 4C) as well as impaired IRS-1 activation (Fig. 4E) in 3XTg-AD mice indicate that this mouse model resembles a central IR-β/LRP-1 defective phenotype (Liu et al., 2015). Our study revealed that HFD feeding further aggravated LRP-1 dysregulation in peripheral (liver; Fig. 3C) and central (brain; Fig. 4D) compartments, however without having significant effects on cerebrovascular LRP-1 levels. Hepatic LRP-1 was reported to regulate insulin signaling and its deletion causes insulin resistance thereby attributing to increased body weight gain, dyslipidemia, glucose intolerance, and low surface IR expression (Au et al., 2017). Since LRP-1 regulates energy homeostasis *via* leptin signaling (Liu et al., 2011a), impaired cerebral and hepatic LRP-1 levels in 3XTg-AD and HFD fed mice may contribute to dysregulated brain and peripheral energy homeostasis. Surprisingly, HFD-induced LRP-1 dysregulation did not affect IR-β levels in brain and liver, indicating that metabolic changes upon HFD feeding independently regulate LRP-1 and IR-β homeostasis.

Under insulin resistant or deprived states as manifest in HFD fed 3XTg-AD mice, insulin may not efficiently regulate LRP-1 expression, thereby contributing to impaired central and peripheral Aβ clearance. Regarding the question on the direction of causation between diabetes and AD, our data support a ‘reverse causation’ with AD driving diabetes, consistent with the development of a vicious cycle between AD and diabetes as proposed by Vandal et al. (2014) based on their findings of glucose intolerance in 3XTg-AD mice resulting from pancreatic human Aβ accumulation and which was rescued by insulin. We here observed a potentially additive vicious cycle in the brain of 3XTg-AD mice, where Aβ production in the brain parenchyma acts on BCEC to reduce both LRP-1 and IR-β, which consequently hampers insulin mediated effects on LRP-1 and Aβ clearance to the periphery. HFD feeding may further worsen central and peripheral Aβ clearance by diminishing pancreatic insulin production and by downregulating LRP-1 levels in central (brain) and peripheral (liver) compartments.

Although the 3XTg-AD mouse model develops cerebral/neuronal Aβ deposition very early (Oddo et al., 2003) as confirmed in the present study by detection of soluble and insoluble brain Aβ levels, 6E10 IF staining, and congo red staining in male and female mice (Fig. 2A–C, Supplement Fig. 5A&B), incidence of cerebral amyloid angiopathy (CAA), predominantly represented by cerebrovascular insoluble Aβ fibril accumulation was not

evident in 9-month-old 3XTg-AD female or male mice (Supplement Fig. 5E–H). However, the cerebrovasculature is known to interact and transport soluble Aβ, predominantly *via* endothelial LRP-1, which is known to regulate about 50% of total brain Aβ clearance in a mouse model of AD (Storck et al., 2016). It is thus conceivable that increased Aβ challenge does occur at the level of the BBB under conditions of early detectable Aβ deposition in brain parenchyma only, as in the present study.

Recent evidences suggest that Aβ peptides induce autophagy in cerebrovascular endothelial cells in mouse (Hayashi et al., 2009) and humans (Rajadas et al., 2013). We observed a profound increase in LC3B-II levels in 3XTg-AD brain lysates indicating active autophagy in 3XTg-AD mice and HFD fed NTg mice (Fig. 6D&E). LC3B and CD31 immune-fluorescent quantification in cerebral vessels revealed a higher number of LC3B dots in male and female 3XTg-AD as compared to NTg mice (Fig. 6A–C) which was further enhanced by HFD feeding in 3XTg-AD but not in NTg mice. Even though HFD feeding elevated LC3B levels in NTg mouse brain, LC3B coverage on cerebral vessels was unchanged compared to chow fed NTg mice (Fig. 6A–E). It is thus conceivable that in 3XTg-AD mice increased Aβ levels correlate with enhanced cerebrovascular LC3B levels and reduced LRP-1 and IR-β receptor levels.

To understand the molecular basis of Aβ driven LRP-1 and IR-β receptor downregulation at the BBB, we investigated the pathways regulating protein turnover and degradation and their impact on Aβ mediated degradation of LRP-1 and IR-β, particularly autophagy-lysosomal proteolysis, also termed autophagy (Fecto et al., 2014). The latter predominantly regulates surface receptor recycling and is next to the ubiquitin-proteasomal pathway primarily involved in degradation of misfolded proteins. We chose to pursue mechanism of Aβ induced autophagy-lysosomal dysregulation using $A\beta_{1–40}$, since this is the most abundant soluble amyloid peptide found in biological fluids and in cerebrovascular amyloid plaques (Hayashi et al., 2009; Zlokovic et al., 1996). Using cultured pBCEC, we identified that Aβ has the ability to induce lysosomes, represented by enhanced cellular LAMP-1 levels and autophagy, represented by elevated levels of LC3B and ATGs (Fig. 8B–D). Using chloroquine (lysosomal inhibitor), we were able to rescue Aβ mediated autophagy-lysosomal degradation of LRP-1 and IR-β proteins in pBCEC. Moreover, chloroquine treatment blunted Aβ induced LAMP-1 upregulation as well as autophagy as indicated by reduced ATG levels, and enhanced LC3B accumulation, suggesting that autophagy-lysosomal degradation is impaired (Fig. 8B–D). MG132 treatment partially rescued LRP-1 and IR-β protein levels, since it affected Aβ induced LAMP-1 activity without affecting autophagy, in fact MG132 induced autophagic flux as indicated by enhanced LC3B-II levels, cytoplasmic inclusions and marginal upregulation of ATGs, which are responsible for autophagophore formation and maturation (Mizushima et al., 2011) (Fig. 8A–D). These findings further explain the earlier reported phenomenon of elevated LC3 and LAMP-1 levels observed in brains of 3XTg-AD mice (Villamil-Ortiz and Cardona-Gomez, 2015).

While it is well established that neuronal LRP1 plays a critical role in Aβ clearance (Kanekiyo et al., 2013), it also influences glucose metabolism and neuronal insulin signaling by regulating IR-β expression (Fuentealba et al., 2009; Liu et al., 2015). However, the role of LRP-1 in cerebrovascular endothelial cell IR-β regulation and its effects on insulin

signaling have been less studied. By employing RNA interference, we found that silencing LRP-1 did affect post-translational regulation of IR-β without affecting mRNA levels (Fig. 9A&B), hence lowered IR-β levels, and impaired insulin-mediated activation of insulin receptor pIR (Tyr1131) and downstream signaling protein pAKT (S473) (Fig. 9C–G). Surprisingly however, IR-β silencing showed no effect on LRP-1 mRNA or protein levels but diminished insulin-mediated IR and AKT activation (Fig. 9C–G). These findings suggest the presence of an imperative cross talk between LRP-1 and IR-β at post-translational level in pBCEC, and that Aβ impairs insulin receptor dynamics and function by accelerating IR-β and LRP-1 degradation at the BBB.

Limitations of the present study may refer to the animal model used. The development of AD pathology in a transgenic, APP over-expressing AD mouse model like 3XTg-AD will not exactly mimic human pathology owing to the heterogeneity and complexity of the disease. Similarly, it is important to remember that HFD feeding is not only a model of diabetes but also of hyperlipidemia, atherosclerosis, and metabolic syndrome. Further studies using more robust models reciprocating human pathology may provide valuable insights regarding the early changes in cerebrovascular LRP-1 and IR-β receptors and their impact on the development and progression of the disease.

In conclusion, our study demonstrates impaired central and cerebromicrovascular IR-β and LRP-1 levels along with impaired central insulin signaling in male and female 3XTg-AD mice with early AD pathology. Changes in cerebrovascular IR-β and LRP-1 levels corresponded with elevated LC3B levels in 3XTg-AD mice. HFD feeding further exacerbated central and peripheral LRP-1 levels independent on changes in IR-β levels at the BBB. Gender variability was observed in food intake which corresponds to body weight gain, Aβ burden, and memory impairment, all elevated in female 3XTg-AD mice compared to their male counterparts. Mechanistic studies conducted in cultured pBCEC revealed that Aβ exposure enhanced IR-β and LRP-1 trafficking to lysosomes and accelerated degradation by inducing autophagy-lysosomal pathways, in turn significantly perturbing insulin mediated responses. LRP-1 deletion post-translationally affected the BBB IR-β turnover and had a significant impact on insulin-mediated responses in pBCEC. Our studies for the first time demonstrate the impact of Aβ burden on BCEC LRP-1 and IR-β homeostasis using *in vitro* and *in vivo* models.

Owing to the therapeutic importance towards drugs targeted to brain LRP-1 (Martiskainen et al., 2013; Storck and Pietrzik, 2017), intranasal insulin therapies (Avgerinos et al., 2018; Craft et al., 2012; de la Monte, 2012), and anti-diabetics (Alagiakrishnan et al., 2013; Cao et al., 2018) to modulate toxic Aβ build-up in the brain and improve memory in mild cognitively impaired AD individuals, our studies using the 3XTg-AD mouse model and *in vitro* porcine BBB model elaborated Aβ mediated mechanisms leading to impairment in cerebrovascular endothelial LRP-1 and IR-β receptors which are primarily involved in Aβ uptake, insulin signaling, and cell metabolism. Targeting these receptors at the level of the BBB to modulate Aβ clearance from brain may provide possible therapeutic intervention in AD.

Supplementary Material

Refer to Web version on PubMed Central for supplementary material.

Acknowledgements

The authors thank Kurt Zatloukal and Meghana Somlapura (Institute of Pathology, Medical University of Graz) for providing antibodies ATG 3&5, PSMD4 and HSP27; Claus U. Pietrzik (Institute for Pathobiochemistry, Johannes Gutenberg-University, Mainz, Germany) for providing LRP-1 (1704) antibody; Pia Benedikt (Institute of Molecular Biosciences, University of Graz, Austria) for providing pIRS-1(S1101) and IRS-1 antibodies. The authors thank Gerhard A. Holzapfel and Anna Pukaluk (Institute of Biomechanics, Graz University of Technology, Austria) for assistance with polarized light microscopy.

Sources of funding

This work was supported by the Austrian Science Fund FWF (DK-MCD W1226 (U.P., D.K.), P24783 (U.P.), and I3535 (A.L.), and the PhD program “Molecular Medicine” of the Medical University of Graz. We further thank BioTechMed-Graz (Flagship Project “Lipases and Lipid Signaling” to A.L. and D.K.).

Abbreviations

3XTg-AD	APP_{Swe}, PSI_{M146V}, tau_{P301L}
AD	Alzheimer's disease
APN/CD13	aminopeptidase N
APP	amyloid precursor protein
ATG3	autophagy-related protein 3
ATG5	autophagy-related protein 5
Aβ	amyloid beta peptide
BBB	blood-brain barrier
BCA	bicinchoninic acid assay
BCEC	brain capillary endothelial cells
BM	Barnes maze
BSA	bovine serum albumin
CAA	cerebral amyloid angiopathy
CSF	cerebrospinal fluid
DEA	diethylamine
FA	formic acid
HCl	hydrochloric acid
HFD	high fat-high cholesterol diet

Europe PMC Funders Author Manuscripts

Europe PMC Funders Author Manuscripts

HFIP	hexafluoro-2-propanol
HPRT-1	hypoxanthine phosphoribosyltransferase 1
HSP27	heat shock protein 27
IB	immuneblotting
IF	immune-fluorescent
IR(s)	insulin receptor(s)
IRS-1	insulin receptor substrate-1
IR-β	insulin receptor beta
KO	knock out
LAMP-1	lysosomal-associated membrane protein 1
LC3B	microtubule-associated proteins 1A/1B light chain 3B
LRP-1	low-density lipoprotein receptor-related protein-1
MAPK	mitogen-activated protein kinase
mBCEC	murine brain capillary endothelial cells
mm	*Mus musculus*
NEFA	non-esterified fatty acids
NTC	non-targeting control
NTg	non-transgenic
OGTT	oral glucose tolerance test
pBCEC	porcine brain capillary endothelial cells
PDGFR-β	platelet-derived growth factor receptor beta
PECAM/CD31	platelet endothelial cell adhesion molecule
PFA	paraformaldehyde
PI3-K	phosphoinositide 3-kinase
PSMD4	26S proteasome non-ATPase regulatory subunit 4
PVDF	polyvinylidene difluoride membrane
RT	room temperature
SF	serum free
sLRP-1	soluble low-density lipoprotein receptor-related protein-1

ss	*Sus scrofa*

References

Alagiakrishnan K, et al. Antidiabetic drugs and their potential role in treating mild cognitive impairment and Alzheimer's disease. Discov Med. 2013; 16:277–286. [PubMed: 24333407]

Attar A, et al. A shortened Barnes maze protocol reveals memory deficits at 4-months of age in the triple-transgenic mouse model of Alzheimer's disease. PLoS One. 2013; 8:e80355. [PubMed: 24236177]

Au DT, et al. The LDL receptor-related protein 1: at the crossroads of lipoprotein metabolism and insulin signaling. J Diabetes Res. 2017; 2017

Avgerinos KI, et al. Intranasal insulin in Alzheimer's dementia or mild cognitive impairment: a systematic review. J Neurol. 2018; 265:1497–1510. [PubMed: 29392460]

Bedse G, et al. Aberrant insulin signaling in Alzheimer's disease: current knowledge. Front Neurosci. 2015; 9:204. [PubMed: 26136647]

Caccamo A, et al. Molecular interplay between mammalian target of rapamycin (mTOR), amyloid-beta, and Tau: effects on cognitive impairments. J Biol Chem. 2010; 285:13107–13120. [PubMed: 20178983]

Caligioni CS. Assessing reproductive status/stages in mice. Curr Protoc Neurosci. 2009; :1–8. DOI: 10.1002/0471142301.nsa04is48

Cao B, et al. Comparative efficacy and acceptability of antidiabetic agents for Alzheimer's disease and mild cognitive impairment: a systematic review and network meta-analysis. Diabetes Obes Metab. 2018; 20:2467–2471. [PubMed: 29790638]

Carroll JC, et al. Sex differences in beta-amyloid accumulation in 3xTg-AD mice: role of neonatal sex steroid hormone exposure. Brain Res. 2010; 1366:233–245. [PubMed: 20934413]

Casali BT, Landreth GE. Abeta extraction from murine brain homogenates. Bio Protoc. 2016; 6

Chirackal Manavalan AP, et al. Phospholipid transfer protein is expressed in cerebrovascular endothelial cells and involved in high density lipoprotein biogenesis and remodeling at the blood-brain barrier. J Biol Chem. 2014; 289:4683–4698. [PubMed: 24369175]

Clinton LK, et al. Age-dependent sexual dimorphism in cognition and stress response in the 3xTg-AD mice. NeuroBiol Dis. 2007; 28:76–82. [PubMed: 17659878]

Craft S, et al. Intranasal insulin therapy for Alzheimer disease and amnestic mild cognitive impairment: a pilot clinical trial. Arch Neurol. 2012; 69:29–38. [PubMed: 21911655]

Deane R, et al. LRP/amyloid beta-peptide interaction mediates differential brain efflux of Abeta isoforms. Neuron. 2004; 43:333–344. [PubMed: 15294142]

Engelman JA, et al. Tumor necrosis factor alpha-mediated insulin resistance, but not dedifferentiation, is abrogated by MEK1/2 inhibitors in 3T3-L1 adipocytes. Mol Endocrinol. 2000; 14:1557–1569. [PubMed: 11043572]

Fecto F, et al. Protein recycling pathways in neurodegenerative diseases. Alzheimers Res Ther. 2014; 6:13. [PubMed: 25031631]

Frank HJ, et al. Binding and internalization of insulin and insulin-like growth factors by isolated brain microvessels. Diabetes. 1986; 35:654–661. [PubMed: 3011572]

Frolich L, et al. Brain insulin and insulin receptors in aging and sporadic Alzheimer's disease. J Neural Transm (Vienna). 1998; 105:423–438. [PubMed: 9720972]

Frolich L, et al. A disturbance in the neuronal insulin receptor signal transduction in sporadic Alzheimer's disease. Ann N Y Acad Sci. 1999; 893:290–293. [PubMed: 10672251]

Fuentealba RA, et al. Low density lipoprotein receptor-related protein 1 promotes anti-apoptotic signaling in neurons by activating Akt survival pathway. J Biol Chem. 2009; 284:34045–34053. [PubMed: 19815552]

Ghasemi R, et al. Repeated intra-hippocampal injection of beta-amyloid 25–35 induces a reproducible impairment of learning and memory: considering caspase-3 and MAPKs activity. Eur J Pharmacol. 2014; 726:33–40. [PubMed: 24418687]

Gray SM, et al. Unravelling the regulation of insulin transport across the brain endothelial cell. Diabetologia. 2017; 60:1512–1521. [PubMed: 28601906]

Griffith CM, et al. Impaired glucose tolerance and reduced plasma insulin precede decreased AKT phosphorylation and GLUT3 translocation in the hippocampus of old 3xTg-AD mice. J Alzheimers Dis. 2019; 68:809–837. [PubMed: 30775979]

Hayashi S, et al. Alzheimer disease-associated peptide, amyloid beta40, inhibits vascular regeneration with induction of endothelial autophagy. Arterioscler Thromb Vasc Biol. 2009; 29:1909–1915. [PubMed: 19815818]

Hirata-Fukae C, et al. Females exhibit more extensive amyloid, but not tau, pathology in an Alzheimer transgenic model. Brain Res. 2008; 1216:92–103. [PubMed: 18486110]

Ito S, et al. Regulation of tight-junction integrity by insulin in an in vitro model of human blood-brain barrier. J Pharm Sci. 2017; 106:2599–2605. [PubMed: 28456720]

Jolivalt CG, et al. Defective insulin signaling pathway and increased glycogen synthase kinase-3 activity in the brain of diabetic mice: parallels with Alzheimer's disease and correction by insulin. J Neurosci Res. 2008; 86:3265–3274. [PubMed: 18627032]

Kanekiyo T, et al. Neuronal clearance of amyloid-beta by endocytic receptor LRP1. J Neurosci. 2013; 33:19276–19283. [PubMed: 24305823]

Kang DE, et al. Modulation of amyloid beta-protein clearance and Alzheimer's disease susceptibility by the LDL receptor-related protein pathway. J Clin Invest. 2000; 106:1159–1166. [PubMed: 11067868]

Kleinridders A, et al. Insulin action in brain regulates systemic metabolism and brain function. Diabetes. 2014; 63:2232–2243. [PubMed: 24931034]

Knight EM, et al. High-fat diet-induced memory impairment in triple-transgenic Alzheimer's disease (3xTgAD) mice is independent of changes in amyloid and tau pathology. NeuroBiol Aging. 2014; 35:1821–1832. [PubMed: 24630364]

Kober AC, et al. Implications of cerebrovascular ATP-binding cassette transporter G1 (ABCG1) and apolipoprotein M in cholesterol transport at the blood-brain barrier. Biochim Biophys Acta. 2017; 1862:573–588.

Kocaturk NM, Gozuacik D. Crosstalk between mammalian autophagy and the ubiquitin-proteasome system. Front Cell Dev Biol. 2018; 6:128. [PubMed: 30333975]

Kucejova B, et al. Hepatic mTORC1 opposes impaired insulin action to control mitochondrial metabolism in obesity. Cell Rep. 2016; 16:508–519. [PubMed: 27346353]

Lilienbaum A. Relationship between the proteasomal system and autophagy. Int J Biochem Mol Biol. 2013; 4:1–26. [PubMed: 23638318]

Liu Q, et al. Neuronal LRP1 knockout in adult mice leads to impaired brain lipid metabolism and progressive, age-dependent synapse loss and neurodegeneration. J Neurosci. 2010; 30:17068–17078. [PubMed: 21159977]

Liu Q, et al. Lipoprotein receptor LRP1 regulates leptin signaling and energy homeostasis in the adult central nervous system. PLoS Biol. 2011a; 9:e1000575. [PubMed: 21264353]

Liu Y, et al. Deficient brain insulin signalling pathway in Alzheimer's disease and diabetes. J Pathol. 2011b; 225:54–62. [PubMed: 21598254]

Liu CC, et al. Neuronal LRP1 regulates glucose metabolism and insulin signaling in the brain. J Neurosci. 2015; 35:5851–5859. [PubMed: 25855193]

Martiskainen H, et al. Targeting ApoE4/ApoE receptor LRP1 in Alzheimer's disease. Expert Opin Ther Targets. 2013; 17:781–794. [PubMed: 23573918]

Matsuzaki T, et al. Insulin resistance is associated with the pathology of Alzheimer disease: the Hisayama study. Neurology. 2010; 75:764–770. [PubMed: 20739649]

Miller DW, et al. Identification and distribution of insulin receptors on cultured bovine brain microvessel endothelial cells: possible function in insulin processing in the blood-brain barrier. J Cell Physiol. 1994; 161:333–341. [PubMed: 7962117]

Mizushima N, et al. The role of Atg proteins in autophagosome formation. Annu Rev Cell Dev Biol. 2011; 27:107–132. [PubMed: 21801009]

Moloney AM, et al. Defects in IGF-1 receptor, insulin receptor and IRS-1/2 in Alzheimer's disease indicate possible resistance to IGF-1 and insulin signalling. NeuroBiol Aging. 2010; 31:224–243. [PubMed: 18479783]

de la Monte SM. Early intranasal insulin therapy halts progression of neurodegeneration: progress in Alzheimer's disease therapeutics. Aging Health. 2012; 8:61–64. [PubMed: 26855666]

Mullins RJ, et al. Insulin resistance as a link between amyloid-beta and tau pathologies in Alzheimer's disease. Front Aging Neurosci. 2017; 9:118. [PubMed: 28515688]

Oddo S, et al. Triple-transgenic model of Alzheimer's disease with plaques and tangles: intracellular Abeta and synaptic dysfunction. Neuron. 2003; 39:409–421. [PubMed: 12895417]

Pardridge WM, et al. Human blood-brain barrier insulin receptor. J Neurochem. 1985; 44:1771–1778. [PubMed: 2859355]

Pitts MW. Barnes maze procedure for spatial learning and memory in mice. Bio Protoc. 2018; 8

Pratchayasakul W, et al. Effects of high-fat diet on insulin receptor function in rat hippocampus and the level of neuronal corticosterone. Life Sci. 2011; 88:619–627. [PubMed: 21315737]

Rajadas J, et al. Enhanced Abeta(1–40) production in endothelial cells stimulated with fibrillar Abeta(1–42). PLoS One. 2013; 8:e58194. [PubMed: 23505467]

Ramanathan A, et al. Impaired vascular-mediated clearance of brain amyloid beta in Alzheimer's disease: the role, regulation and restoration of LRP1. Front Aging Neurosci. 2015; 7:136. [PubMed: 26236233]

Sagare A, et al. Clearance of amyloid-beta by circulating lipoprotein receptors. Nat Med. 2007; 13:1029–1031. [PubMed: 17694066]

Sartorius T, et al. The brain response to peripheral insulin declines with age: a contribution of the blood-brain barrier? PLoS One. 2015; 10:e0126804. [PubMed: 25965336]

Shibata M, et al. Clearance of Alzheimer's amyloid-ss(1–40) peptide from brain by LDL receptor-related protein-1 at the blood-brain barrier. J Clin Invest. 2000; 106:1489–1499. [PubMed: 11120756]

Steen E, et al. Impaired insulin and insulin-like growth factor expression and signaling mechanisms in Alzheimer's disease–is this type 3 diabetes? J Alzheimers Dis. 2005; 7:63–80. [PubMed: 15750215]

Storck SE, Pietrzik CU. Endothelial LRP1 - apotential target for the treatment of Alzheimer's disease: theme: drug discovery, development and delivery in Alzheimer's disease guest editor: Davide Brambilla. Pharm Res. 2017; 34:2637–2651. [PubMed: 28948494]

Storck SE, et al. Endothelial LRP1 transports amyloid-beta(1–42) across the blood-brain barrier. J Clin Invest. 2016; 126:123–136. [PubMed: 26619118]

Subramaniam S, Unsicker K. ERK and cell death: ERK1/2 in neuronal death. FEBS J. 2010; 277:22–29. [PubMed: 19843173]

Swaminathan SK, et al. Insulin differentially affects the distribution kinetics of amyloid beta 40 and 42 in plasma and brain. J Cereb Blood Flow Metab. 2017; 0(0):1–15. DOI: 10.1177/0271678X17709709

Takeda S, et al. Diabetes-accelerated memory dysfunction via cerebrovascular inflammation and Abeta deposition in an Alzheimer mouse model with diabetes. Proc Natl Acad Sci U S A. 2010; 107:7036–7041. [PubMed: 20231468]

Talbot K, et al. Demonstrated brain insulin resistance in Alzheimer's disease patients is associated with IGF-1 resistance, IRS-1 dysregulation, and cognitive decline. J Clin Invest. 2012; 122:1316–1338. [PubMed: 22476197]

Tamaki C, et al. Major involvement of low-density lipoprotein receptor-related protein 1 in the clearance of plasma free amyloid beta-peptide by the liver. Pharm Res. 2006; 23:1407–1416. [PubMed: 16779710]

Tamaki C, et al. Insulin facilitates the hepatic clearance of plasma amyloid beta-peptide (1 40) by intracellular translocation of low-density lipoprotein receptor-related protein 1 (LRP-1) to the plasma membrane in hepatocytes. Mol Pharmacol. 2007; 72:850–855. [PubMed: 17609417]

Vandal M, et al. Insulin reverses the high-fat diet-induced increase in brain Abeta and improves memory in an animal model of Alzheimer disease. Diabetes. 2014; 63:4291–4301. [PubMed: 25008180]

Vandal M, et al. Age-dependent impairment of glucose tolerance in the 3xTg-AD mouse model of Alzheimer's disease. FASEB J. 2015; 29:4273–4284. [PubMed: 26108977]

Velazquez R, et al. Central insulin dysregulation and energy dyshomeostasis in two mouse models of Alzheimer's disease. NeuroBiol Aging. 2017; 58:1–13. [PubMed: 28688899]

Villamil-Ortiz JG, Cardona-Gomez GP. Comparative analysis of autophagy and tauopathy related markers in cerebral ischemia and Alzheimer's disease animal models. Front Aging Neurosci. 2015; 7:84. [PubMed: 26042033]

Werther GA, et al. Localization and characterization of insulin receptors in rat brain and pituitary gland using in vitro autoradiography and computerized densitometry. Endocrinology. 1987; 121:1562–1570. [PubMed: 3653038]

Yang GY, et al. Induction of focal angiogenesis through adenoviral vector mediated vascular endothelial cell growth factor gene transfer in the mature mouse brain. Angiogenesis. 2003; 6:151–158. [PubMed: 14739621]

Yang Y, et al. Intranasal insulin ameliorates tau hyperphosphorylation in a rat model of type 2 diabetes. J Alzheimers Dis. 2013; 33:329–338. [PubMed: 22936005]

Zandl-Lang M, et al. Regulatory effects of simvastatin and apoJ on APP processing and amyloid-beta clearance in blood-brain barrier endothelial cells. Biochim Biophys Acta. 2018; 1863:40–60.

Zenaro E, et al. Neutrophils promote Alzheimer's disease-like pathology and cognitive decline via LFA-1 integrin. Nat Med. 2015; 21:880–886. [PubMed: 26214837]

Zeng Y, et al. Cerebral insulin, insulin signaling pathway, and brain angiogenesis. Neurol Sci. 2016; 37:9–16. [PubMed: 26442674]

Zhao Z, et al. Central role for PICALM in amyloid-beta blood-brain barrier transcytosis and clearance. Nat Neurosci. 2015; 18:978–987. [PubMed: 26005850]

Zlokovic BV, et al. Glycoprotein 330/megalin: probable role in receptor-mediated transport of apolipoprotein J alone and in a complex with Alzheimer disease amyloid beta at the blood-brain and blood-cerebrospinal fluid barriers. Proc Natl Acad Sci U S A. 1996; 93:4229–4234. [PubMed: 8633046]

Europe PMC Funders Author Manuscripts

Europe PMC Funders Author Manuscripts

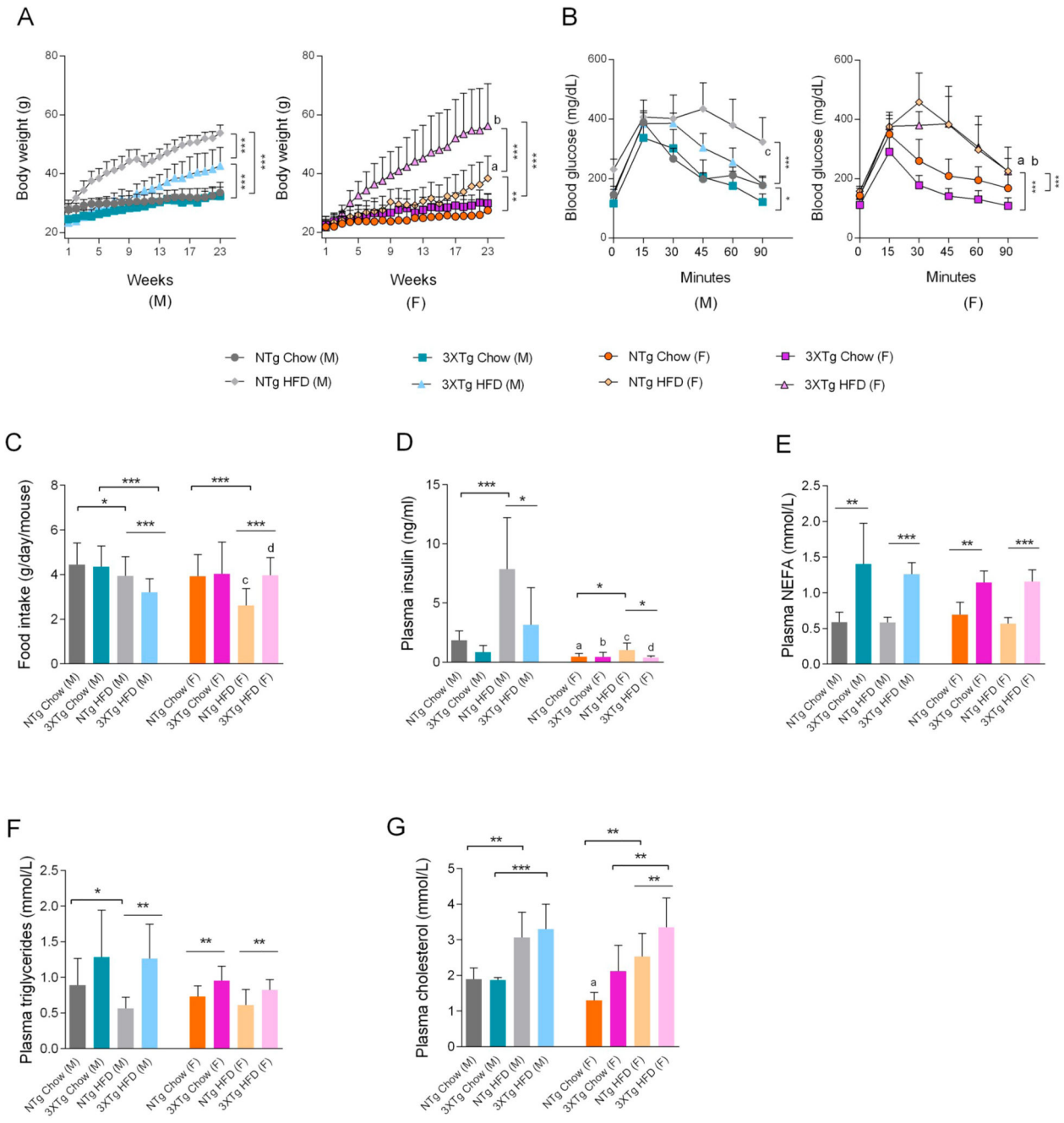

Fig. 1.

Dysregulated metabolic profile in 3XTg-AD and HFD-fed mice. (A) Animal body weights were monitored every week until the end of the 23 weeks feeding regimen. Data represent mean ± SD; (N = 7–10 mice/group/sex). Two-way ANOVA was performed, $^{**}p < 0.01$ and $^{***}p < 0.001$. Comparison between NTg HFD (M) *vs* NTg HFD (F) ($^{a}p < 0.001$) and NTg HFD (F) *vs* 3XTg-AD HFD (F) ($^{b}p < 0.001$). (B) Oral glucose tolerance test (OGTT) was performed in mice fasted for 6 h. Data represent mean ± SD; (N = 7–10 mice/group/sex). Two-way ANOVA was performed, $^{*}p < 0.05$ and $^{***}p < 0.001$. Comparison between NTg

HFD (M) *vs* NTg HFD (F) ($^{a}p < 0.05$), 3XTg-AD chow (M) *vs* 3XTg-AD chow (F) ($^{b}p < 0.05$) and NTg HFD (M) *vs* 3XTg-AD HFD (M) ($^{c}p < 0.05$). (C) Daily food intake. After 23 weeks of feeding, animals were fasted, plasma was isolated and plasma parameters such as (D) insulin, (E) non esterified fatty acids (NEFA), (F) triglycerides (TG), and (G) cholesterol were determined as described in material and methods. For C, D, E, F and G, statistical differences between the groups were evaluated using two-tailed, unpaired students *t*-test. Data represent mean ± SD; N = 7–9 mice/group, except for the 3XTg-AD male chow fed group, where $N = 4$ mice, $*p < 0.05$, $**p < 0.01$ and $***p < 0.001$. Comparison between the sexes was performed using two-tailed, unpaired students *t*-test (NTg chow (M) *vs* NTg chow (F); $^{a}p < 0.001$), (3XTg-AD chow (M) *vs* 3XTg-AD chow (F); $^{b}p < 0.05$), (NTg HFD (M) *vs* NTg HFD (F); $^{c}p < 0.001$) and (3XTg-AD HFD (M) *vs* 3XTg-AD HFD (F); $^{d}p < 0.001$).

Europe PMC Funders Author Manuscripts

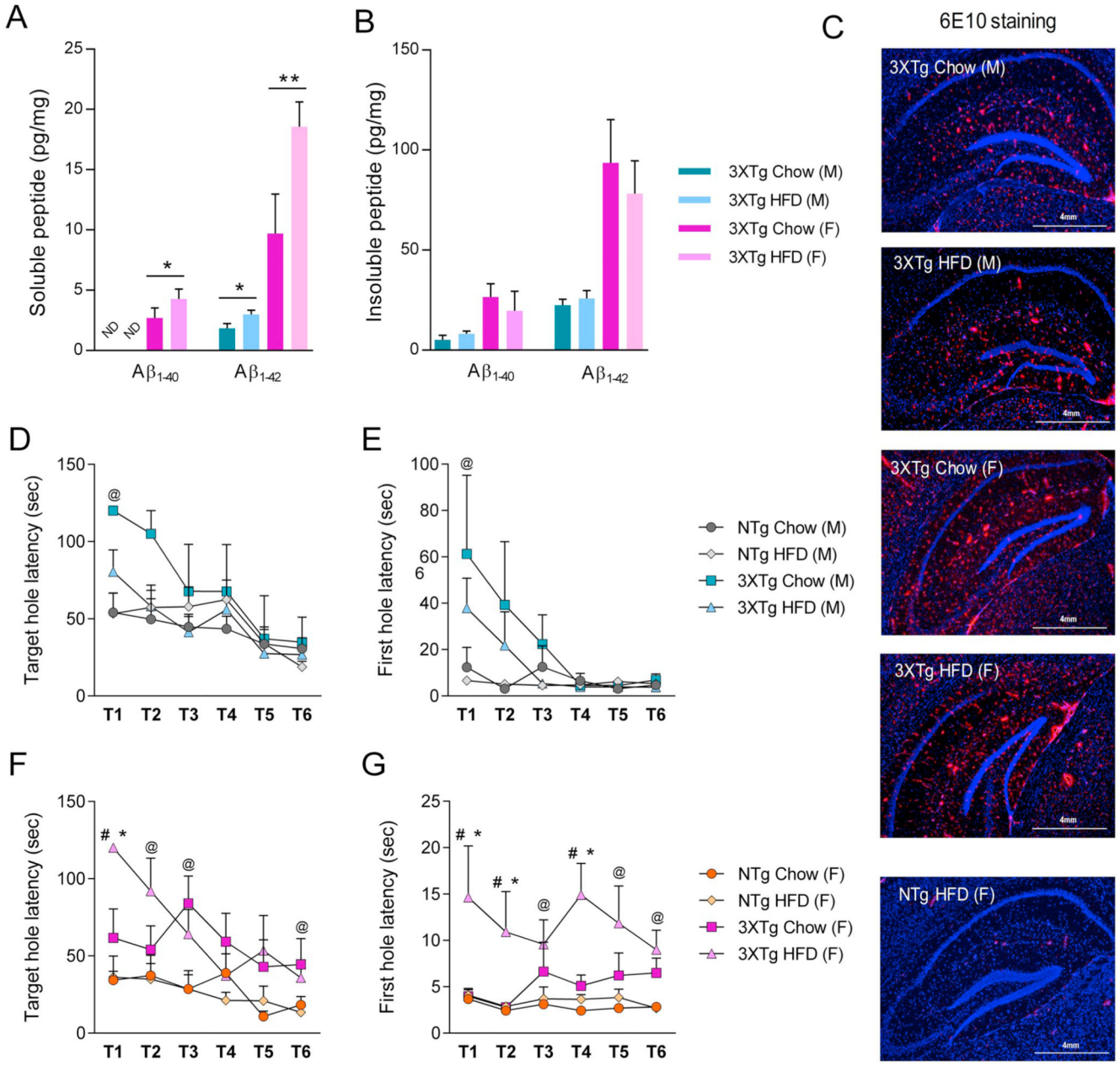

Fig. 2.

Effect of HFD feeding, gender, and 3XTg-AD transgene on cerebral Aβ burden and memory. Soluble and insoluble Aβ was extracted from the cortices of 3XTg-AD mice. (A, B) Levels of diethylamine soluble ('soluble') and formic acid soluble (i.e. 'insoluble') human $A\beta_{1-40}$ and $A\beta_{1-42}$ in total brain parenchyma of chow and HFD-fed 3XTg-AD mice, quantified by ELISA ($N = 4$ mice per group). Data represent means ± SD. Statistical significance was determined using two-tailed, unpaired students *t*-test (*$p < 0.05$ and **$p < 0.01$). C) Representative immune-fluorescent staining of Aβ burden in the hippocampus of chow and HFD fed 3XTg-AD and NTg, male and female mice. DAPI staining in blue, 6E10 staining in red. (D–G) At the end of 20 weeks during the course of HFD feeding animals

were tested for anxiety and memory using Barnes Maze (BM). (D, F) Target hole latency (memory), (E, G) First hole latency (anxiety). $N = 8$ mice/group, except for 3XTg-AD male chow fed, where $N = 4$ mice/group. Data represent mean ± SEM. $^{@}p < 0.05$ for main effect: 3XTg-AD *vs* NTg independently of diet; $^{*}p < 0.05$ *vs* NTg/chow; $^{\#}p < 0.05$ *vs* 3XTg-AD chow fed mice. (For interpretation of the references to colour in this figure, the reader is referred to the web version of this article.)

Europe PMC Funders Author Manuscripts

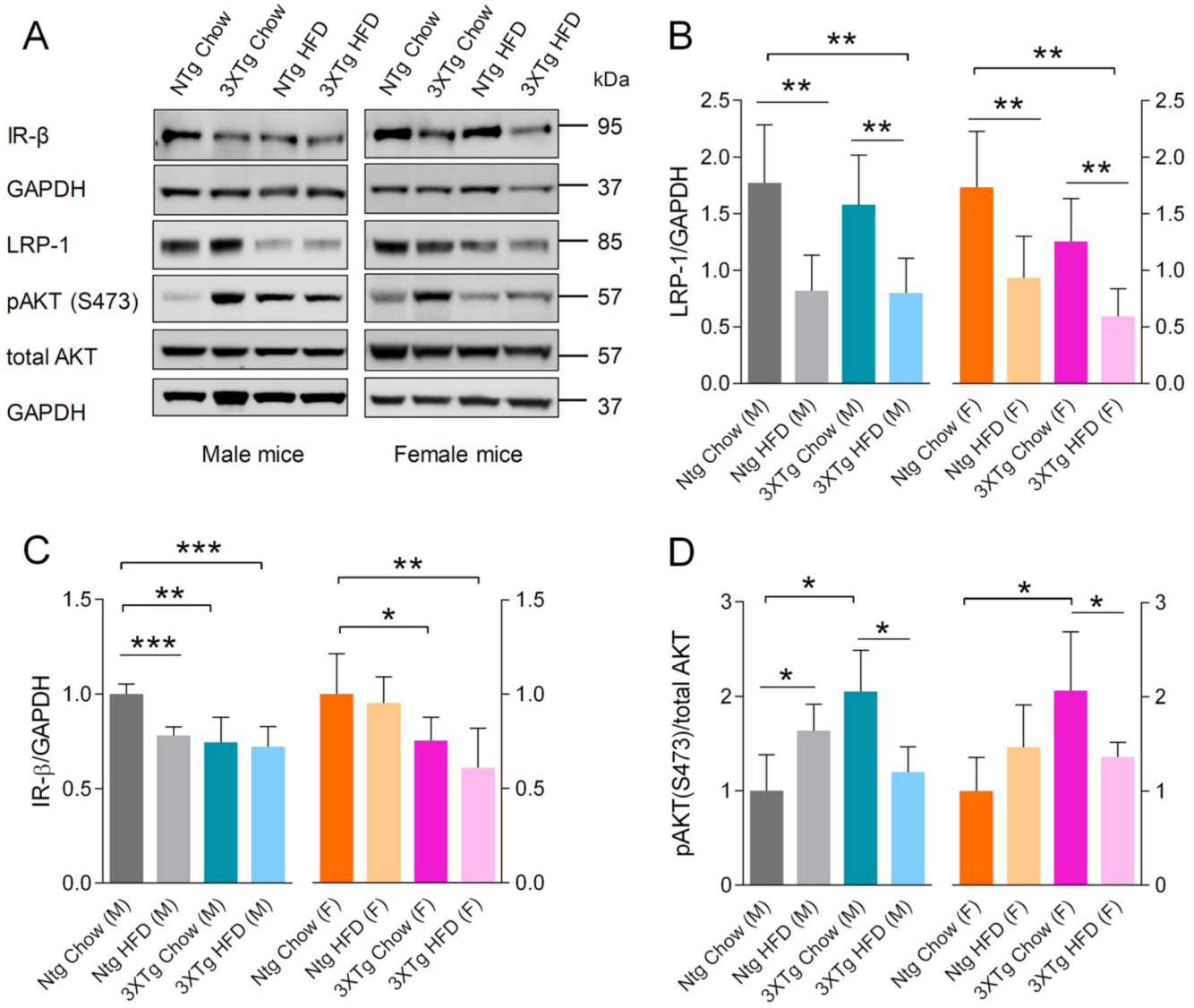

Fig. 3.

Effect of HFD feeding and 3XTg-AD transgene on liver IR-β/LRP-1 axis. At the end of the feeding regimen (23 weeks), liver lysates were prepared from mice of both genotypes and genders, and were subjected to immune-blotting using polyclonal antibodies. (A) Representative blots for IR-β, LRP-1, pAKT(s473), total AKT and GAPDH. Quantitative, densitometric analysis of (B) LRP-1 ($N = 5$) and (C) IR-β ($N = 5$). Intensities of respective bands were normalized to GAPDH used as loading control. Quantitative, densitometric analysis of (D) pAKT(s473) ($N = 4$). Intensities of pAKT(s473) bands were normalized to total AKT. Data represent mean ± SD. Statistically significant differences between the groups were calculated using two-tailed, unpaired students *t*-test. *$p < 0.05$, **$p < 0.01$ and ***$p < 0.001$.

Europe PMC Funders Author Manuscripts

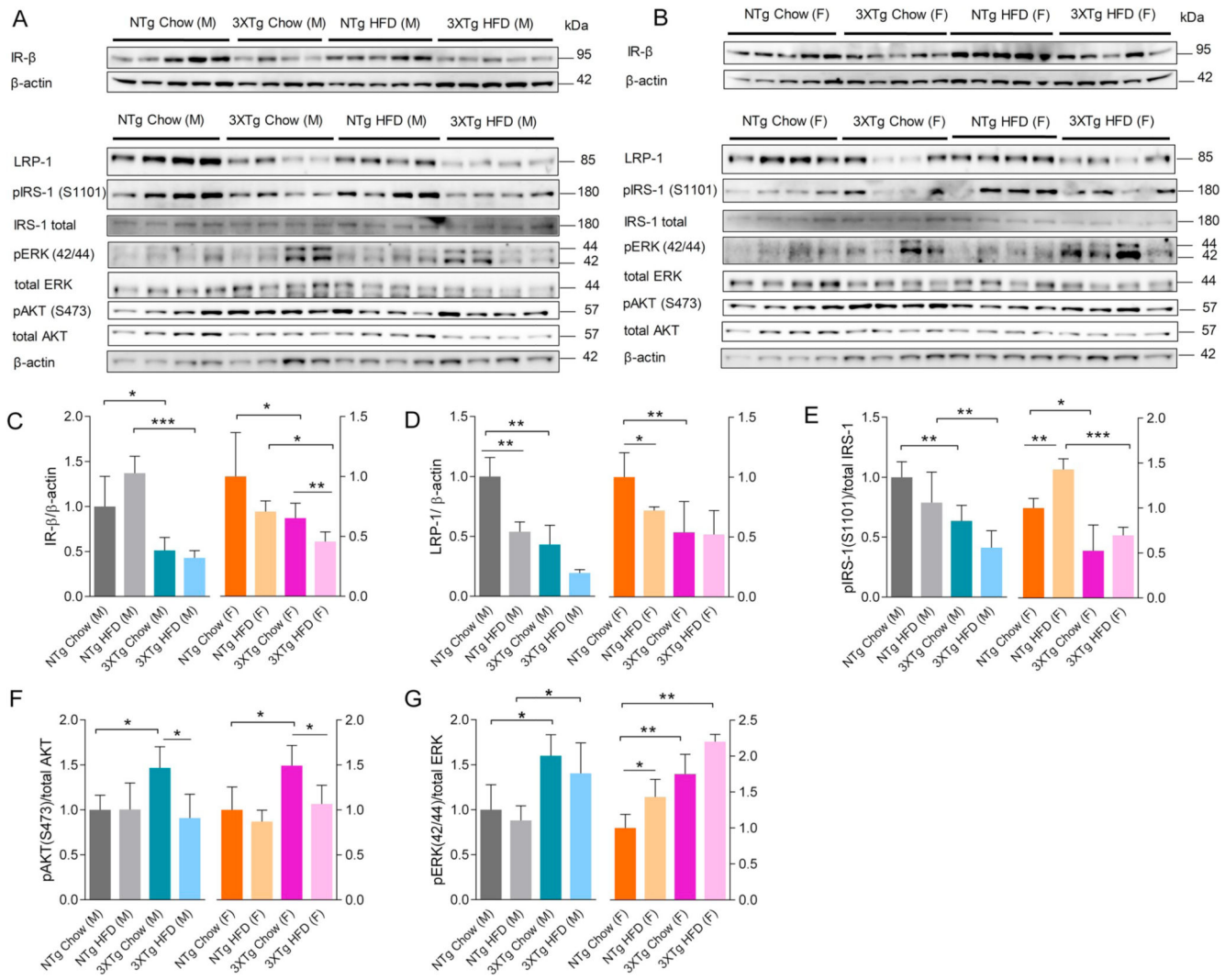

Fig. 4.

Effects of HFD feeding and 3XTg-AD transgene on brain IR-β/LRP-1 axis and downstream insulin signaling. Immunoblot analyses of brain lysates were performed and changes in IR-β/LRP-1 levels and insulin signaling events were analyzed using specific antibodies. A, B: Representative immune-blots for brain IR-β, LRP-1, pIRS-1(S1101), IRS-1, pERK(42/44), ERK, pAKT, total AKT and β-actin levels in male and female mice of both the genotypes. Densitometric analysis of specific bands for (C) IR-β ($N = 5$) and (D) LRP-1 ($N = 5$) as normalized to β-actin. Quantitative analysis of (E) pIRS-1(S1101) (N = 5), (F) pAKT(s473) ($N = 5$) and (G) pERK ($N = 5$), where band intensities were normalized to respective total protein band intensities. Data represent mean ± SD. Statistically significant differences between groups were calculated using two-tailed, unpaired students *t*-test. $*p < 0.05$, $**p < 0.01$, and $***p < 0.001$.

Europe PMC Funders Author Manuscripts

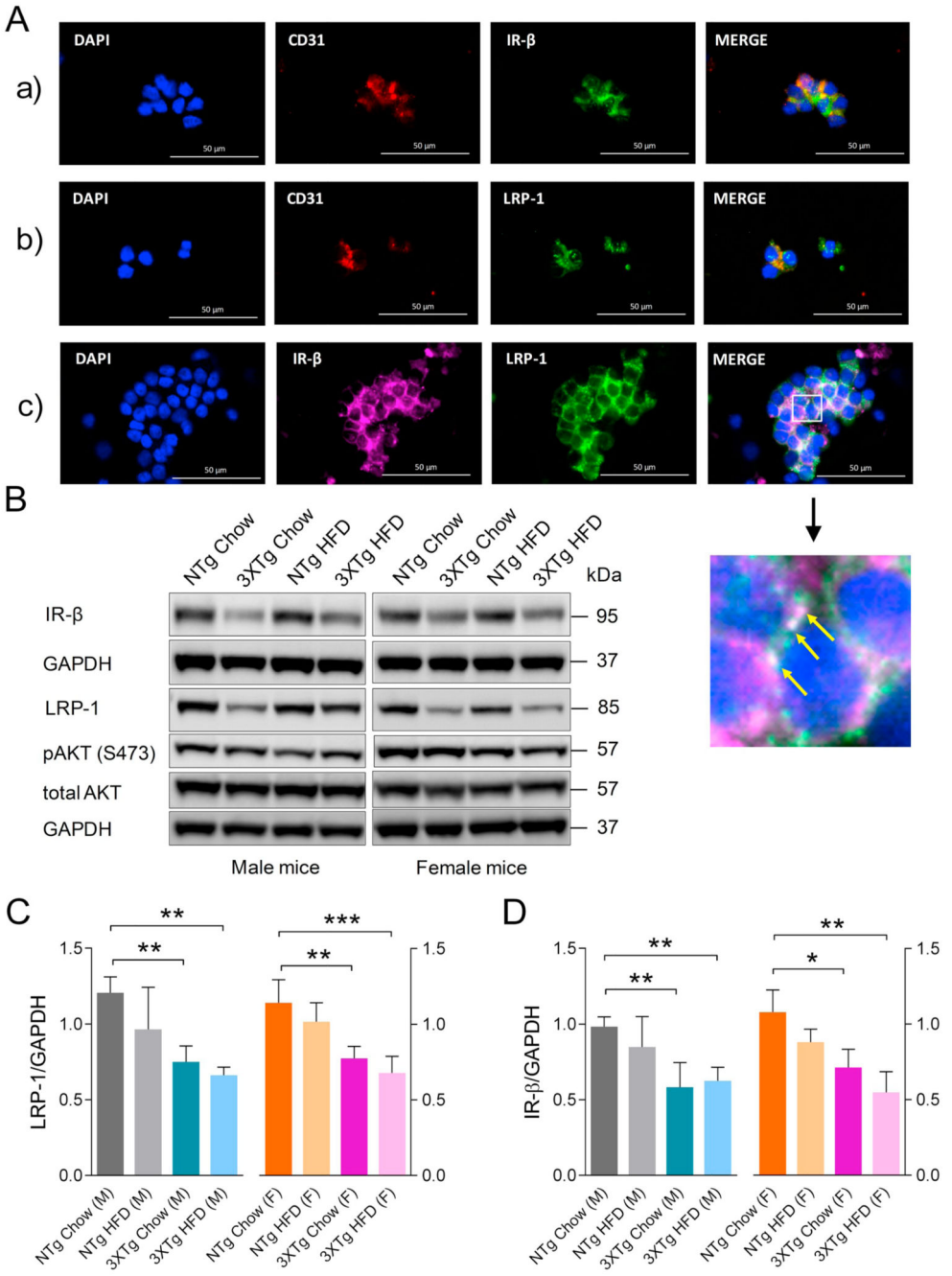

Fig. 5.

Perturbed IR-β/LRP-1 axis at the BBB in 3XTg-AD mice. At the end of the HFD feeding period (23 weeks), fasted animals were sacrificed. Cerebromicrovasculature was isolated as described in Material and methods. (A) IR-β and LRP-1 presence in mBCEC. Isolated cerebral microvessels were immune-fluorescently stained for (a) CD31 (red) and IR-β (green); (b) CD31 (red) and LRP-1 (green); (c) IR-β (magenta) and LRP-1 (green). DAPI (nuclear stain) staining in blue. Co-localization of IR-β and LRP-1, shown in white, represented by yellow arrows. (B-D) Murine BCEC protein lysates of male and female

3XTg-AD and NTg mice of both feeding regimens were subjected to immunoblot analyses. (B) Representative blots for IR-β, LRP-1, pAKT, total AKT and GAPDH levels. Densitometric analysis of specific bands for (C) IR-β ($N = 4$) and (D) LRP-1 ($N = 4$) as normalized to GAPDH as loading control. Data represent mean ± SD; significant differences between the groups were calculated using two-tailed, unpaired students *t*-test; *$p < 0.05$; **$p < 0.01$ and ***$p < 0.001$. (For interpretation of the references to colour in this figure, the reader is referred to the web version of this article.)

Europe PMC Funders Author Manuscripts

Europe PMC Funders Author Manuscripts

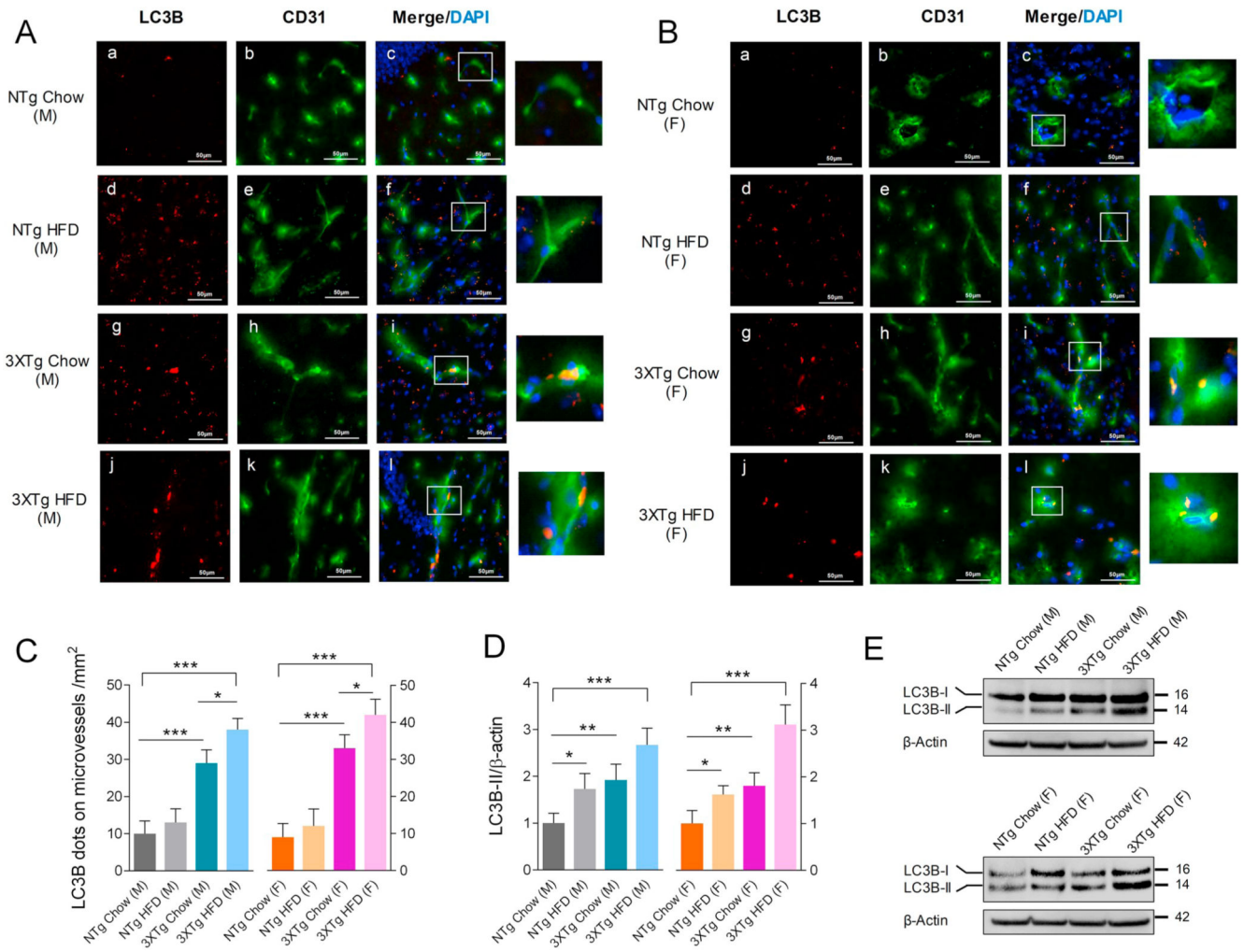

Fig. 6.

LC3B levels are elevated in brain and cerebrovascular endothelium in 3XTg-AD mice. LC3B (red) and CD31 (green) double immune-fluorescent labeled 18 μM cryosections of brains from (A) male and (B) female HFD and chow fed mice of both genotypes, DAPI stain in blue represents nuclear stain. White boxes indicate areas of LC3B and CD31 protein colocalization (yellow) in the cerebrovasculature. (C) Bar diagram depicting quantification of LC3B dots covering the vessels in 1mm^2 sections in cortical cryosections of male and female mice of both genotypes and feeding conditions. $N = 3$ animals per group. Data represent mean ± SD values; for statistical evaluation one-way ANOVA was applied, followed by Dunnett's post-hoc test and intra species evaluation was done using student's unpaired *t*-test; *$p < 0.05$ and ***$p < 0.001$. (D) Densitometric evaluation of LC3B-II levels normalized to β-actin in brain lysates. $N = 3$ samples per group, Data represent mean ± SD; statistical evaluation was made using one-way ANOVA, followed by Dunnett's post-hoc test; *$p < 0.05$; **$p < 0.01$ and ***$p < 0.001$. (F) Representative immune-blots for LC3B and β-actin in mouse brain lysates. (For interpretation of the references to colour in this figure legend, the reader is referred to the web version of this article.)

Europe PMC Funders Author Manuscripts

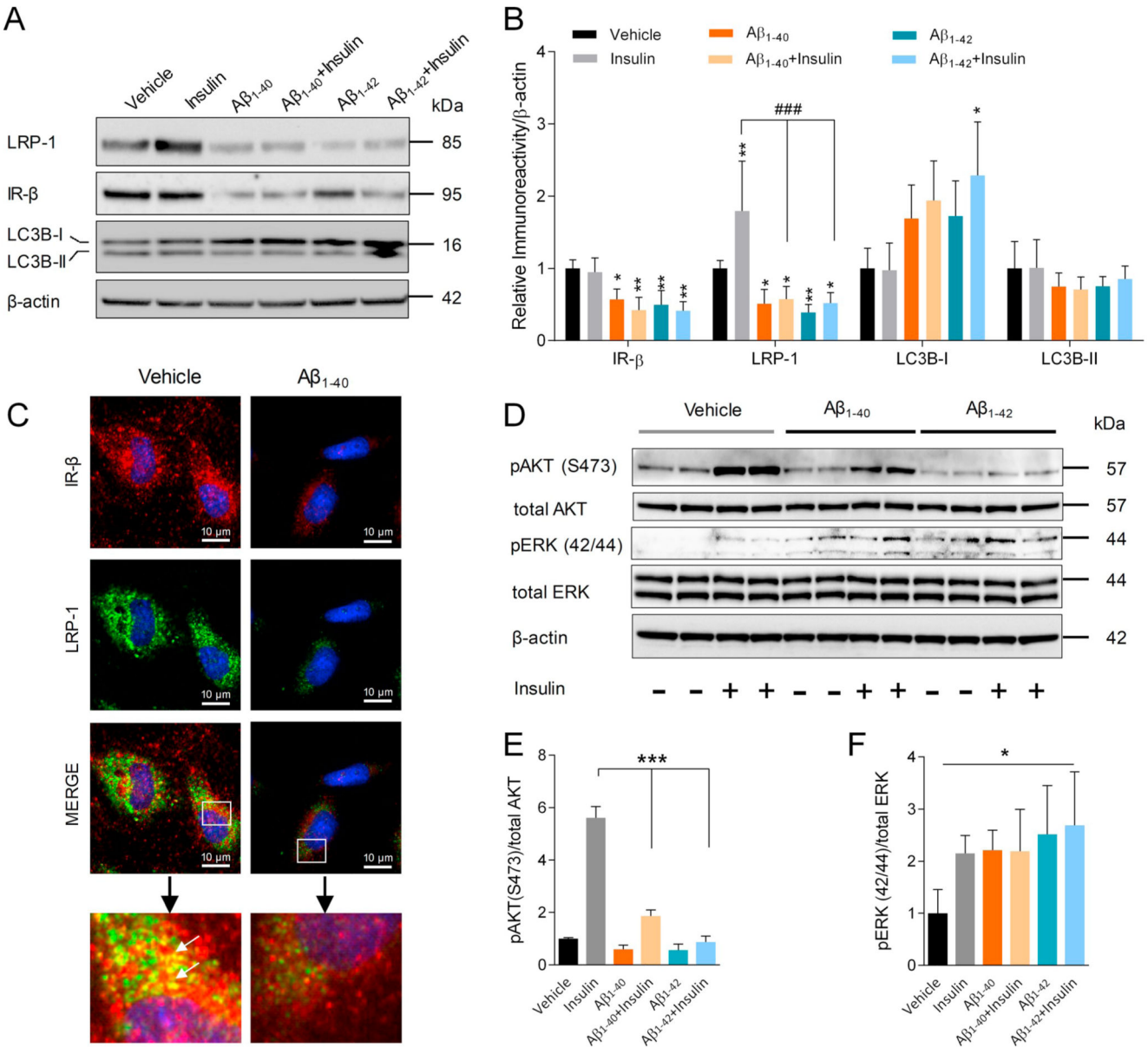

Fig. 7.

Effect of Aβ isoforms on insulin induced LRP-1 and IR-β levels and insulin mediated signaling in pBCEC. Serum starved primary pBCEC were probed with insulin (100 nM) with or without $A\beta_{1–40}$ or $A\beta_{1–42}$ peptides (240 nM) for 6 h, and total cell lysates were subjected to immune-blotting. (A) Representative immune-blots for LRP-1, IR-β, and LC3B expression. (B) Densitometric evaluation of LRP-1, IR-β, LC3B-II and LC3B-I levels Relative band intensities were normalized to β-actin; $n = 3$ experiments from different cell preparations performed in duplicates. One-way ANOVA followed by Dunnett's post-hoc test was used; $^{*}p < 0.05$ and $^{**}p < 0.01$ *vs* vehicle treatment; $^{\#\#\#}p < 0.001$ *vs* insulin treatment. (C) Cells were incubated with either vehicle or $A\beta_{1–40}$ peptide (240 nM) for 6 h under serum free conditions, washed, fixed with 4% PFA, probed with antibodies against LRP-1

(green) and IR-β (red) to visualize the receptor interaction (yellow). (D-F) Cells were treated with vehicle (0.01 N HCL and 1% NH_4OH), insulin (100 nM), $A\beta_{1–40}$ or $A\beta_{1–42}$ peptides (240 nM), or a combination of insulin and $A\beta_{1–40}$ or $A\beta_{1–42}$ for 30 min. Cell lysates were prepared and subjected to IB using specific primary antibodies.(D) Representative immune-blots for pAKT, total AKT, pERK, total ERK and β-actin. Quantitative analysis of (E) pAKT and (F) pERK, normalized to their respective total protein levels; $n = 4$ experiments from different cell preparations performed in duplicates. Data represent mean ± SD. Statistically significant differences were calculated using one-way ANOVA, followed by Dunnett's post-hoc test. *$p < 0.05$, **$p < 0.01$, and ***$p < 0.001$. (For interpretation of the references to colour in this figure, the reader is referred to the web version of this article.)

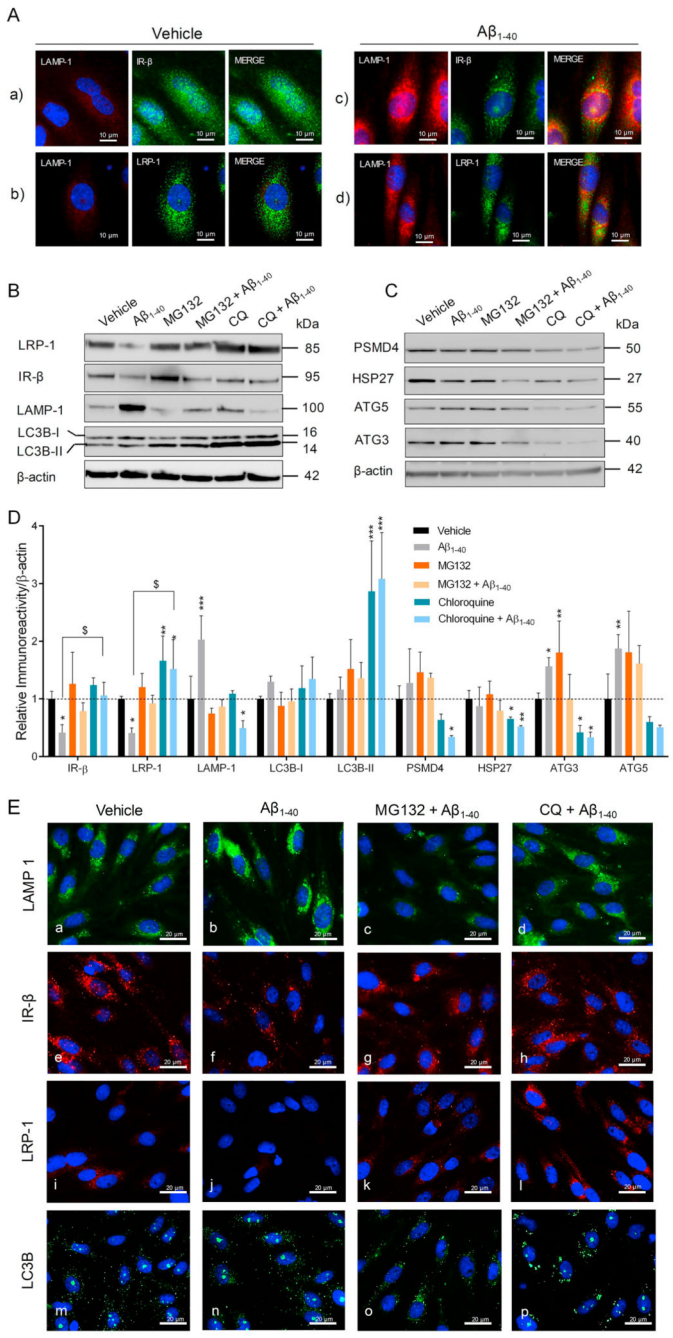

Fig. 8.

Aβ aggravates LRP-1 and IR-β degradation by inducing autophagy-lysosomal activity in pBCEC. Freshly isolated pBCEC were seeded on collagen-G coated 6 well plates and coated chamber slides. Cells were serum starved for 6 h and incubated with vehicle or freshly reconstituted $A\beta_{1–40}$ (240 nM) for 6 h. (A) Double immune-fluorescent stainings of (a, c) LAMP-1 (red) and IR-β (green), (b, d) LAMP-1 (red) and LRP-1 (green). (B–D) Cells were incubated with vehicle or $A\beta_{1–40}$ (240 nM), with or without chloroquine (30 μM) and MG132 (20 μM) for 6 h under serum free conditions, lysed and subjected to immune-

Europe PMC Funders Author Manuscripts

blotting (B, C) Representative immune-blots for LRP-1, IR-β, LAMP-1, LC3B, PSMD4, HSP27, ATG5, and ATG3 protein expression. (D) Densitometric evaluation of the proteins listed in B, C. Band intensities were normalized to β-actin. Data represent mean ± SD of 3 independent experiments performed in duplicates. Statistically significant differences were calculated using one-way ANOVA, followed by Dunnett's post-hoc test (*$p < 0.05$, **$p < 0.01$, and ***$p < 0.001$) and unpaired students *t*-test ($^{\$}p < 0.05$). (E) Cells were treated with $A\beta_{1–40}$ peptide with or without chloroquine (30 μM) and MG132 (20 μM) for 6 h, 4% PFA fixed and immune-fluorescently stained with LAMP-1 (green; a–d), IR-β (red; e–h), LRP-1 (red; i–l) and LC3B (green; m–p). Nuclear staining (DAPI) in blue. (For interpretation of the references to colour in this figure, the reader is referred to the web version of this article.)

Europe PMC Funders Author Manuscripts

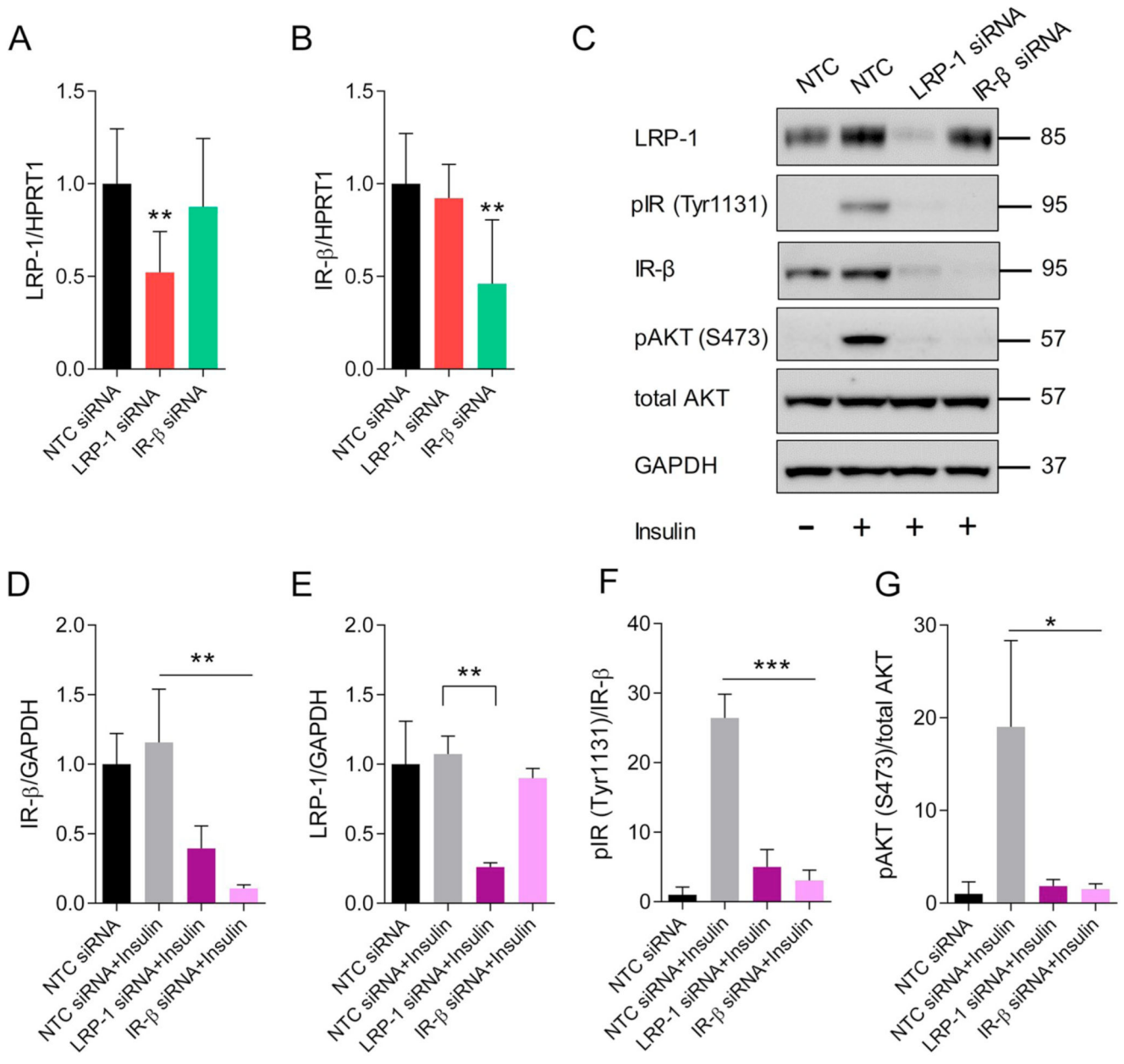

Fig. 9.

LRP-1 regulates IR-β expression by modulating its post-translational modification in pBCEC. Specific gene silencing in pBCEC was achieved by RNA interference using either NTC siRNA, LRP-1 siRNA, or IR-β siRNA for 48 h. Gene silencing efficiency was confirmed by subjecting isolated cDNA to RT-qPCR. (A) LRP-1 mRNA levels and (B) IR-β mRNA levels, normalized to HPRT1. $n = 3$ independent experiments performed in triplicates. Statistically significant differences were calculated using one-way ANOVA, followed by Dunnett's post-hoc test; *$p < 0.05$; **$p < 0.01$ and ***$p < 0.001$. Silenced cells were serum starved for 12 h and treated with either vehicle (0.01 N HCL) or insulin (100 nM solubilized in 0.01 N HCL) for 5 min to induce pIR (Tyr1131) and pAKT (S473). After

incubation, cells were lysed, and proteins were subjected to IB using respective antibodies. (C) Representative immune-blots for LRP-1, pIR (Tyr1131), IR-β, pAKT (S473), total AKT and GAPDH. (D-G) Quantitative densitometric analysis of (D) IR-β and (E) LRP-1 band intensities,normalized to GAPDH; quantitative analysis of (F) pAKT (S473) and (G) pIR (Tyr1131), where the band intensities were normalized to respective total protein band intensities. Data represents mean ± SD of 3 independent experiments using different cell isolations performed in triplicates. Statistically significant differences were calculated using one-way ANOVA, followed by Dunnett's post-hoc test; *$p < 0.05$; **$p < 0.01$ and ***$p < 0.001$.

Europe PMC Funders Author Manuscripts